

## CHAPTER 1

# *Carbon Nanostructures: Drug Delivery and Beyond*

AGNIESZKA GAJEWSKA<sup>a</sup>, AKCAN ISTIF<sup>a</sup>, JASRA GUL<sup>a,b</sup>,  
MICHELE CHIRONI<sup>a</sup>, ANDREA FAIDIGA<sup>a</sup>, MARCO ROCCO<sup>a</sup>,  
KETTY SLAVEC<sup>a</sup>, TERESA GIANFERRARA<sup>a</sup> AND  
TATIANA DA ROS<sup>\*a</sup>

<sup>a</sup>Department of Chemical and Pharmaceutical Sciences, University of Trieste, Trieste, Italy; <sup>b</sup>International Center for Chemical and Biological Sciences (ICCBS), University of Karachi, Karachi, Pakistan

\*E-mail: [daros@units.it](mailto:daros@units.it)

## 1.1 Introduction

Since the discovery of fullerenes in 1985, the family of carbon nanostructures has widened a lot and nowadays it includes nanotubes, nanodiamonds, nanooxions, nanoribbons, nanocones, nanohorns, graphene and its direct derivatives, as graphene quantum dots, and carbon dots. Despite the fact that they all present interesting characteristics, in the last few years the most studied, from a biological point of view, are carbon nanotubes (CNTs), graphene oxide (GO), graphene quantum dots (GQDs), carbon quantum dots (CQDs) and carbon nanodiamonds (NDs). In fact, lately the interest for fullerenes has dramatically decreased, affecting the number of studies on their properties, but there are still brilliant examples of their biological potential as reported by various authors.<sup>1</sup>

One of the most explored bio-applications of carbon nanostructures is related to their capability to load different payloads and to cross the cellular

---

Nanoscience & Nanotechnology Series No. 48

Carbon Nanostructures for Biomedical Applications

Edited by Tatiana Da Ros, Nazario Martín and Jean-Francois Nierengarten

© The Royal Society of Chemistry 2021

Published by the Royal Society of Chemistry, [www.rsc.org](http://www.rsc.org)

membrane, allowing the intracellular delivery of drugs into cells. Here we will discuss some of the most recent developments in this field, except for fullerenes, which have been recently widely reviewed.<sup>2</sup>

## 1.2 Carbon Nanotubes

CNTs consist of one or several concentric graphene sheets rolled up in a cylindrical shape with a range in diameter from 0.4 nm up to 100 nm. They have been studied from many different aspects.

The biological applications of CNTs are strongly dependent on all of the health hazards that this new material can cause. For several years, the effects of CNTs in cells and tissues have been explored by *in vivo* and toxicological studies. However, it turned out that many parameters of CNTs, (as contaminants, surface chemistry, processing methods, agglomerate states, length, diameter and more) can have various toxic effects.

As was reported, the toxic effect of CNTs can arise not directly from them, but from the residues produced during the synthetic process as nickel, cobalt or iron nanoparticles, which can remain in the CNTs and generate reactive oxygen species (ROS) in a biological environment. It turns out that ROS cause inflammatory symptoms and induce mitochondrial membrane degradation, depletion of antioxidant agents, rise in inflammatory biomarkers, and decreases cell viability. It has been demonstrated that 30% of iron in SWCNTs is able to generate free radicals within 15 min of exposure to epidermal keratinocytes in the presence of DMPO (5,5-dimethyl-1-pyrroline-1-oxide).<sup>3</sup> In a later study it was shown that higher amounts of catalyst generate higher concentrations of free radicals and increase inflammatory responses.<sup>4</sup> Additionally, nickel alters the expression of the gene encoding the protein HIF1A, a factor of transcript involved in the regulation of inflammatory genes and apoptosis.<sup>5</sup> All studies on the toxicity of CNTs must take into account the nature of the metallic catalyst and its percentage/quantity. It is difficult to obtain pure CNTs by removing all traces of catalysts and several methods can be employed to decrease residual catalysts including centrifugation, high-temperature annealing<sup>6</sup> and oxidation treatment by acid reflux.<sup>7</sup>

Toxicity can be also influenced by the modification on the CNTs' surface. Only with acid-treatment on the CNTs' surface is it possible to introduce a number of defect sites along the CNTs' surface (as mentioned earlier). Muller *et al.* changed the number of defect sites on MWCNTs by mechanical grinding and annealing at high temperature and demonstrated that acute pulmonary toxicity and genotoxicity increased after intratracheal administration of MWCNTs with a larger number of defect sites.<sup>8</sup> However, another study by Kagan *et al.* showed that oxidized SWCNTs can be biodegraded more easily by myeloperoxidase enzyme, found in neutrophils and macrophages. The enzyme interacts with carboxylic sites on the nanotubes' surface<sup>9</sup> and oxidized CNTs may be more biocompatible than pristine CNTs from this point of view. Following this pathway, Sayes and co-workers examined cell viability in the presence of oxidized and phenylated tubes. They discovered that the phenylated tubes exhibit lower toxicity, and this can be due to the hindering of the defect sides of the tubes.<sup>10</sup> Dumortier *et al.* have examined the toxicity of CNTs functionalized by

1,3-dipolar cycloaddition. They concluded that CNTs, fully soluble in aqueous culture media, did not modify primary immune cells viability *in vitro*.<sup>11</sup> Also, the CNTs' surface area and their hydrophobic nature have an impact on the toxicity. The tubes, in fact, can potentially interact with several molecules like proteins, RNA, DNA and enzymes with toxic effects on the biological environment.<sup>12</sup> Dutta and co-workers found that the bovine or human serum albumin adsorption onto the CNT surface resulted in inflammatory responses after uptake by macrophage cells. Normally that effect occurs only when albumin adopts structural changes or becomes damaged.<sup>13</sup> The effect of functionalization of the tubes highlights the importance of assessing the toxicity profile for every type of new CNT modification.

Finally, the CNTs' length cannot be ignored. CNT sizes have an important effect on clearance. The length can range from nanometers up to millimeters. The exposure to long fiber-like material can induce dangerous damages in DNA and genetic mutations over a period of exposure, causing an extremely malignant form of cancer, mesothelioma. Symptoms of these bio-persistent fibers are the granulomas, which are the signs of oxidative stress, causing excessive fibrous tissue.<sup>14</sup>

Macrophage are the cells responsible for the removal of foreign material like CNTs from living organisms. Fibers with a length exceeding 20  $\mu\text{m}$  are extremely resistant to phagocytosis<sup>15</sup> and Poland *et al.* have shown that CNTs as spherical or stellate shaped agglomerates with less than 20  $\mu\text{m}$  have no significant damaging reactions compared to samples with individualized MWCNTs, agglomerates, and ropes of MWCNTs with lengths exceeding 20  $\mu\text{m}$ .<sup>14</sup> CNTs can be toxic, but many solutions exist, to moderate or eliminate adverse effects arising from the mentioned problems. In conclusion, CNTs should be used without the presence of metal catalysts, have an appropriate functionalization for the planned purpose with low surface oxidation, present a covered surface to effectively escape bio-interactions and be short to avoid long retention times.

To approach their potential application and effect on humans, pharmacokinetics and biodistribution in animal models have been and are currently being explored, and they depend on numerous factors such as chemical-physical characteristics, solubility, surface functionalization, aggregation of the derivatives themselves,<sup>16</sup> while CNT excretion is mainly renal.<sup>17</sup>

The possible biomedical applications of CNTs span many fields. One example is regenerative medicines due to their biocompatibility, resistance, and possible functionalization of their surface with biomolecules as collagen fibers to form a nanomaterial capable of acting as a scaffold in tissue regeneration, as already reported many years ago.<sup>18</sup> Another potentiality, not properly unraveled up to now, is their supposed antioxidant activity. If this function could be confirmed, they could also be used in the prevention of aging and preservation of food.<sup>19</sup> However, the most promising and studied application for CNTs is delivery systems. In fact, they can be loaded with different pharmaceutical ingredients and be delivered at specific sites, with prolonged accumulation into targeted tissues and reduced prospective systemic toxic effects.<sup>20</sup> The latter aspect is of particular importance in the case of anticancer drugs, the mechanism of action of which is mainly related to their toxic effects

(i.e. alkylation, DNA intercalation, tubulin aggregation/disaggregation equilibrium unbalance among others). In this context, CNTs propose an opportunity to capsule anticancer drugs, thus reducing their toxicity for an organism and enhancing local accumulation in the targeted site.<sup>21</sup> Moreover, it is important to remember that, with the proper modification, it is possible to stimulate the drug release from the drug-CNT complex only in a tumor environment, for example, by lowering the pH under the physiological value (Figure 1.1).<sup>22</sup>

Their capability to act as efficient vehicles for the transport of many molecules is related to their ability to enter into cells, mainly with two mechanisms,<sup>23</sup> one of which—the so-called nano-needle process—is not invasive for biological membranes, considering that the tubes pierce through the phospholipidic double layer without disrupting the surface.<sup>23b</sup> This internalization method could also play a role in the application of CNTs in vaccines.<sup>24</sup> The uptake mechanism, however, depends on various factors such as length, size, nature of functional groups and hydrophobicity (Figure 1.2).<sup>25</sup>

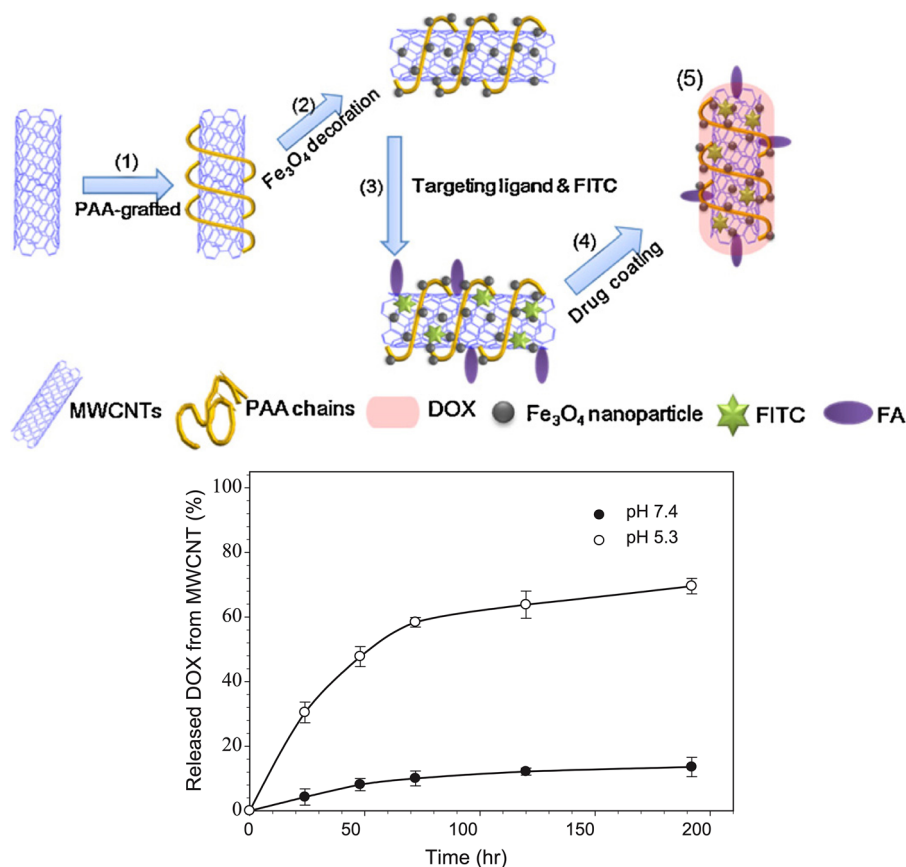


**Figure 1.1** *Top:* Preparation of Fe<sub>3</sub>O<sub>4</sub> magnetic nanoparticles decorated poly(acrylic acid)-grafted MWCNTs, covalently linked to folic acid and fluorescein (steps 1–3) and embedding doxorubicin by non-covalent interactions. *Bottom:* doxorubicin release profile at acid and neutral pH at 37 °C. Adapted from ref. 22 with permission from Elsevier, Copyright 2012.

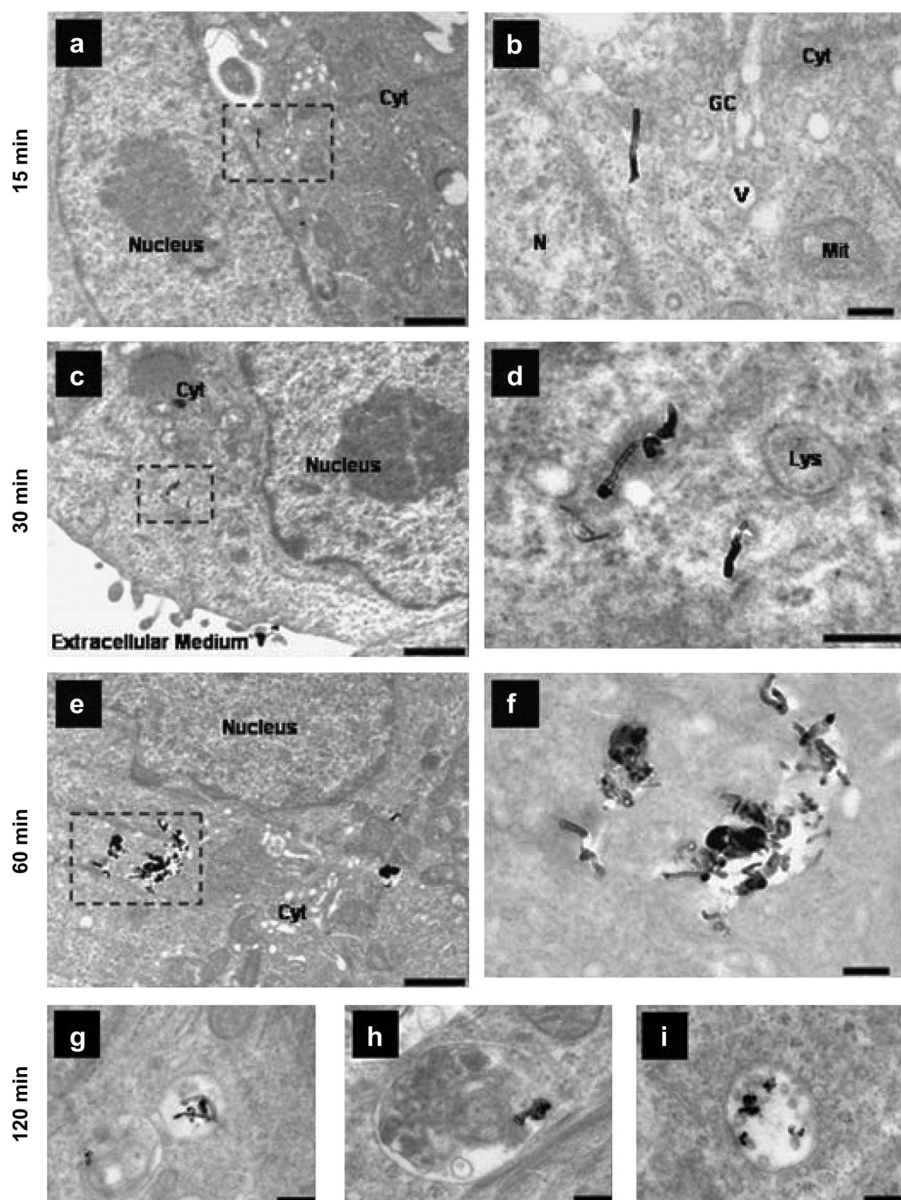


**Figure 1.2** Distribution of functionalized MWCNTs into A549 cells at different time of incubation. Scale bars: 1  $\mu$ m in a, c and e; 200 nm in b, d, f, g, h and i. Cyt, cytoplasm; N, nucleus; GC, Golgi complex; V, vesicle; Mit, mitochondria; Lys, lysosome. Reproduced from ref. 25 with permission from Elsevier, Copyright 2012.

### 1.2.1 CNTs as Cellular Substrates

One of the very promising and important implementations of CNTs is connected with their topological and chemical structure. It is well established that topographies and patterns can influence cellular behaviors. By controlling the nanoscale topography of cellular substrates, the implantation of medical devices facilitates new biological processes, including embryogenesis, angiogenesis and pathological conditions.

CNTs as nanoparticles are inherently appropriate for surface modifications by simple incorporation or deposition on their surface. They have a fibrillar shape and versatile optical, electrical and mechanical characteristics for applications as a cellular substrate. Many groups have successfully utilized CNTs for cellular growth surfaces to provide structural support or present novel properties.<sup>26</sup> For instance, a range of cell phenotypes have shown high binding affinities for CNT surfaces, demonstrating that CNTs may be used for a variety of tissue implantation devices or novel substrates.<sup>27</sup>

Several papers have presented CNTs as conducive to neuronal adhesion and safe for neural processes outgrowth, suggesting that CNTs are biocompatible with neurons. Cellot *et al.* reported that CNTs provide a shortcut for the electrical signaling connecting tight junctions adhered onto the nanotube surface at proximal and distal portions of the neuron.<sup>28</sup> Mature neuronal cells have also been derived directly from human embryonic stem cells (hESCs) using polymer-grafted CNT thin film scaffolds.<sup>29</sup> Malarkey and co-workers, by modulating the thickness and the conductivity of a CNT film, were able to change neuron morphology, neurite outgrowth and the number of growth cones.<sup>30</sup> Even if, until now, neuronal interfacing has no direct clinical benefits, research developments in this area may help to explain biological mechanisms and neural interactions relevant to injury and disease. Preferential interactions of neural cells and CNTs permit the study of axonal outgrowth and connection between neural clusters and patterned CNTs. Also, the directed growth and migration along CNT surface architectures allowed the study of their role to prevent and repair nerve injuries, such as spinal cord injury or stroke.<sup>31</sup>

Lee *et al.* pretreated rats with amine-modified SWCNTs, and they found a protection effect on neurons as well as an improvement in the recovery of behavioral functions in rats with induced stroke. Authors suggest that CNTs with positive charges may have contributed to a favorable environment for neurons.<sup>32</sup> Roman *et al.* investigated the administration of PEGylated SWCNTs after traumatic neural cord injury, which could promote regeneration of axons into the lesion cavity and functional recovery of the hindlimbs.<sup>33</sup> They found that, after a spinal cord injury (SCI), neurofilament-positive fibers of SWCNT-PEG induced a modest improvement in hindlimb locomotor recovery without causing hyperalgesia. These data suggest that SWCNT-PEG may be an effective material to promote axonal repair and regeneration after SCI.

By functionalization, CNTs can be conjugated with imaging agents, such as metallic nanoparticles, quantum dots, or isotopes to make imaging possible *via* conventional techniques. Chen *et al.* studied the conjugation of

CNTs with super paramagnetic iron oxide nanoparticles (SPIO) and NIR fluorescent quantum dots CdTe.<sup>34</sup> The CNTs-SPIO-CdTe nanohybrids exhibited the superparamagnetic behavior of SPIO with a saturation magnetization of about  $65 \text{ emu g}^{-1}$  at room temperature and strong emission band located at a near-infrared wavelength of 734 nm. Different authors used magnetic resonance imaging (MRI) for visualizing CNTs in cells<sup>35</sup> or living organisms<sup>36</sup> taking advantage of the presence of iron oxide impurities.

Recent studies on the application of CNTs for radiotherapy reported several examples of CNTs as a radioisotope carrier. In the case of encapsulation of the radionuclides, Hong *et al.* presented single-walled CNTs filled with sodium iodide-125 (Auger and  $\gamma$ -emitter) for *in vitro* and *in vivo* study.<sup>37</sup> The material had a specific tissue accumulation (lung) and the leakage of the radionuclide was not observed. More recent studies proposed the use of nanocapsules bearing radioactive samarium salt, that can be used both in diagnostics and in therapy, as a new tool for theranostic applications.<sup>38</sup>

### 1.2.2 CNTs as Drug Delivery Systems

As already mentioned, CNTs can be internalized by cells and, by presenting a high surface area, they are ideal to transport a number of compounds on their surface. Their potentiality as drug delivery systems have been explored in depth,<sup>39</sup> with special attention paid to vehiculation for anticancer drugs, a case in which selectivity is a major necessity.

Internalization selectivity can be achieved by exploiting different specific transporters and receptors. A successful approach has been reported by using CNTs decorated with fructose, exploiting glucose transporter (GLUT) receptor-mediated pathways, in particular GLUT5, which is a membrane protein transporting fructose into the cytoplasm.<sup>40</sup> The authors reported a functionalization of CNTs using block copolymer, in which doxorubicin was also introduced. Both covalent and supramolecular approaches were used to decorate the tubes and in the same case also folic acid was introduced to exploit FA receptors for cellular internalization in breast cancer. Tumor breast cancers, in fact, overexpress FA receptors and GLUT5.

The combination of nanotubes, functionalized with folic acid and doxorubicin, with silk protein leads to an injectable hybrid silk hydrogel with enhanced strength resistance due to the presence of carbon nanomaterials. This construct was also able to selectively target the cells overexpressing FA receptors and deliver anthracycline due to the degradation of the silk, with enhancement of the release using NIR pulsed irradiation to trigger the local increase of temperature that helps the detachment of the drug.<sup>41</sup>

In drug delivery studies with CNTs, anthracyclines, such as doxorubicin, are probably the most used drugs<sup>39</sup> because they have very attractive anticancer compounds but they present important cardiotoxic side-effects. Consequently, the idea of decreasing this toxicity by means of a proper vehiculation is very appealing. Moreover, these compounds present aromatic structures, permitting an efficient loading on the tubes also with

strategies that are not covalent, and their fluorescence allowed one to follow directly the fate of the drugs. These studies have been recently summarized in a review.<sup>42</sup>

Pemetrexed, a folic acid analog anti-metabolite anticancer, and/or quercetin, endowed also with proapoptotic activity, were allowed to interact with MWCNTs to obtain three different complexes, bearing one of the two compounds or both at the same time, respectively. The release of pemetrexed and quercetin was investigated at acidic and neutral pH, with better results at pH 7.4, as well as the antitumoral activity on human breast adenocarcinoma cells (MDA-MB-231) and pancreatic cells (PANC-1), demonstrating that there is a synergic effect of pemetrexed and quercetin in PANC-1 cells.<sup>43</sup> With an analogous supramolecular approach, also a complex with tamoxifen was prepared. In this case, however, the drug was entrapped on the nanotubes' surface by a subsequent wrapping of the MWCNTs with lentinan, a biocompatible polysaccharide, that confers water solubility to the complex. This complex was efficiently taken up into cells, inducing enhanced cytotoxicity in human breast adenocarcinoma MCF-7 cells, when combined with the hyperthermia obtained by photoirradiation of the tubes.<sup>44</sup>

Theoretical calculation of the interaction of 5-Fluorouracil (5-FU) with carbon nanotubes was performed finding a good stability.<sup>45</sup> Analogously, the interactions between gemcitabine and pyrrolidine functionalized SWCNTs were explored finding a favorable binding of the drug to the tubes also due to the presence of H bonds with the pyrrolidine nitrogen.<sup>46</sup>

PEGylated MWCNTs were loaded also with another anti-metabolite compound, gemcitabine, and hyaluronic acid, to test the *in vitro* drug release of the anticancer drug, with a good profile. The complex showed a lower hemolytic effect than the drug itself and *in vivo* experiments demonstrated a significant reduction of the tumor and an ameliorated survival with respect to the free drug treatment.<sup>47</sup> Gemcitabine was also combined with MWCNTs and lentinan, a polysaccharide derived from mushrooms, with the aim of associating the chemotherapeutic approach with photothermal treatment, due to the presence of the tubes. These can be irradiated in the NIR and release energy as heat, with local increase of temperature that can kill the cells. The ternary complex CNT-gemcitabine-lentinan was demonstrated to be more effective than the CNTs, the free drug or the CNT-drug construct. Moreover, combination with the local irradiation allows one to obtain a specific enhanced effect only into tumor cells.<sup>48</sup>

Another classical anticancer drug, paclitaxel, was linked to SWCNTs through the interposition of a pH sensitive linker, with the ability to release paclitaxel in the tumor environment. Selective targeting was possible due to the presence of a specific antibody, CD44. The *in vitro* and *in vivo* studies were conducted also in combination with salinomycin, that is known to eradicate cancer stem cells, conjugated to the nanotubes with a PEG chain as well. The results showed an increased efficacy in suppressing the tumor when both the constructs were simultaneously used (Figure 1.3).<sup>49</sup>

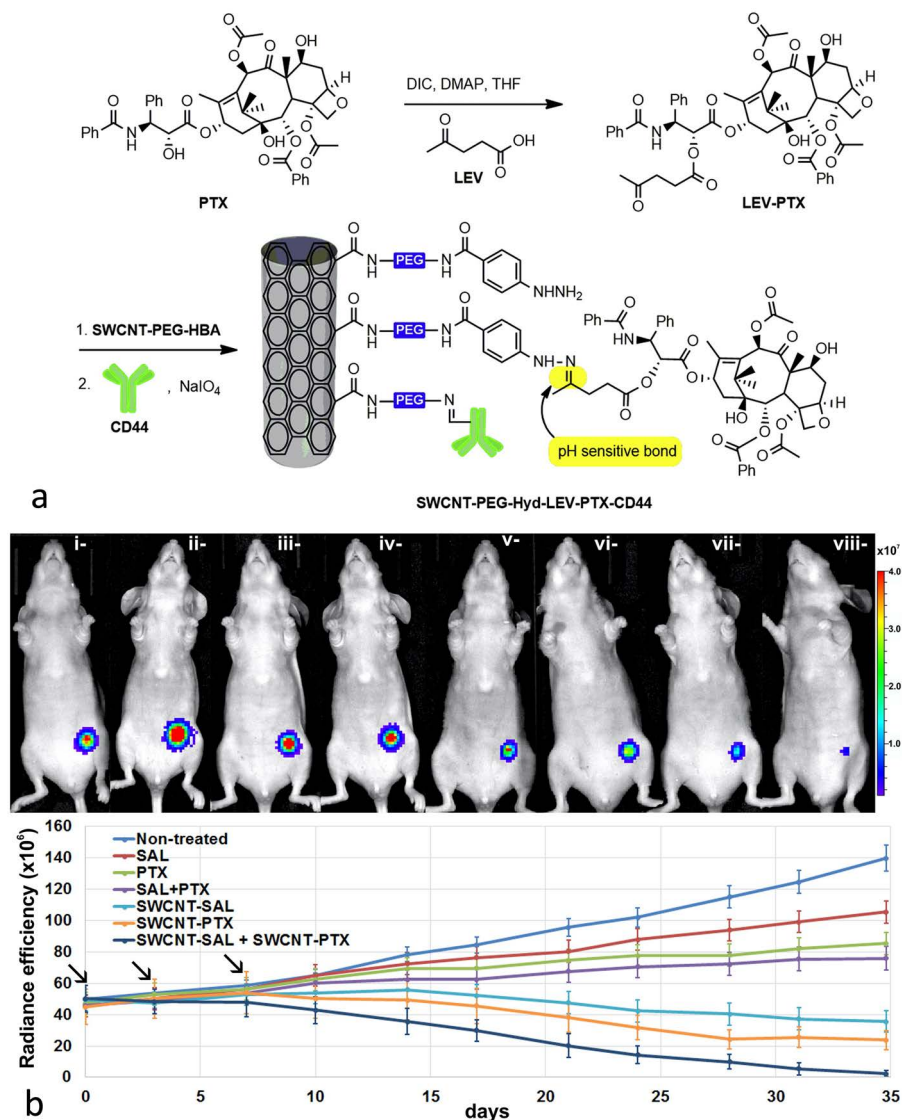


**Figure 1.3** *Panel a*: Preparation of MWCNTs decorated with paclitaxel using a pH sensitive bond (hydrazone) and CD44 antibodies, as selective targeting agent. *Panel b, top*: bioluminescence intensity in *in vivo* experiment in MDA-MB-231 tumor-bearing mice. *Panel b, bottom*: radiance efficiency, corresponding to the tumor volume, at different times. The arrows indicate the injections of the materials. The evaluated mice groups are non-treated mice (Non-treated); treated with salinomycin (SAL); treated with paclitaxel (PTX); treated with a combination of salinomycin and paclitaxel (SAL + PTX); treated with salinomycin-conjugated SWCNTs (SWCNT-SAL); treated with paclitaxel-conjugated SWCNTs (SWCNT-PTX); treated with a combination of salinomycin-conjugated and paclitaxel-conjugated SWCNTs (SWCNT-SAL + SWCNT-PTX). Data expressed as mean  $\pm$  SD,  $n = 3$  per group. Adapted from ref. 49 with permission from Elsevier, Copyright 2016.

With the same aim of killing cancer stem cells, Berber *et al.* explored the synergistic effect of polybenzimidazole-decorated MWCNTs in combination with Pt nanoparticles. The latter release cytotoxic Pt ions in acidic conditions and the proposed scaffold was demonstrated to be very efficient as anticancer.<sup>50</sup>

Another antitumor platinum-based drug, oxaliplatin, was used to design a double functionalized MWCNTs-based drug delivery system, in which also the *trans*-activating transcriptional activator (TAT) was introduced, obtaining a copolymeric structure using polyethylenimine. The presence of the TAT was finalized to the enhancement of the permeability of brain endothelial cells, ameliorating the blood-brain barrier (BBB) penetration, and the construct was able to induce a higher production of ROS, with consequent high efficacy in killing tumor cells in *in vivo* glioma models.<sup>51</sup>

As mentioned, BBB is an important obstacle in delivering drugs to CNS, and the studies to overcome it are of the utmost interest. Recently a nanotube-based construct has been proposed, conjugating on the carbon surface ribavirin, as an antiviral compound, and an opportunely selected nanobody against nervous necrosis virus. The experiments on cells demonstrated that there is a much higher cellular uptake when the nanobody is present with respect to the control system without it and *in vivo* experiments on zebrafish highlighted that the antibody portion allowed concentration of the preparation into the brain (Figure 1.4), with a decrease of infected larvae mortality.<sup>52</sup>

In another study, three different bisphosphonates were covalently conjugated to oxidized MWCNTs to obtain an efficient vehiculation of the antitumor compounds, the use of which usually requires high dosages to reach an efficient effect, but these doses, at the same time, trigger toxic mechanisms. With the aim of finding a better delivery system, drug release from the decorated CNTs was studied at three pH (1.2, 5.5, 7.4) obtaining different kinetics profiles. However, the activities of the CNT-bisphosphonates conjugates on MCF7 cells were not conclusive, in fact the behaviors of the three derivatives were very different from each other (from an increase to a dramatic loss of activity).<sup>53</sup>

As mentioned, studies in the field of drug delivery have been very active<sup>42</sup> for many years. After exploring the combination of CNTs with the most classical anticancer drugs, a lot of work has been done recently on alternative or novel molecules with potentiality in tumor therapy.

Mangiferin, a polyphenolic C-glycoside, is a new anticancer drug with a poor bioavailability that limits its use. In order to improve this aspect, MWCNTs were used to conjugate this compound through the interposition of PEG chains. The proposed system demonstrated better bioavailability and at the same time an ameliorated cytotoxic effect *versus* U-87 glioma cells.<sup>54</sup>

As recently reviewed,<sup>55</sup> formononetin, a chromen-4-one richly present in legumes, clovers and herbs, shows a significant cytotoxicity potentially useful for the treatment of cancers because it induces apoptosis triggering the loss of the mitochondrial membrane potential. This molecule has been

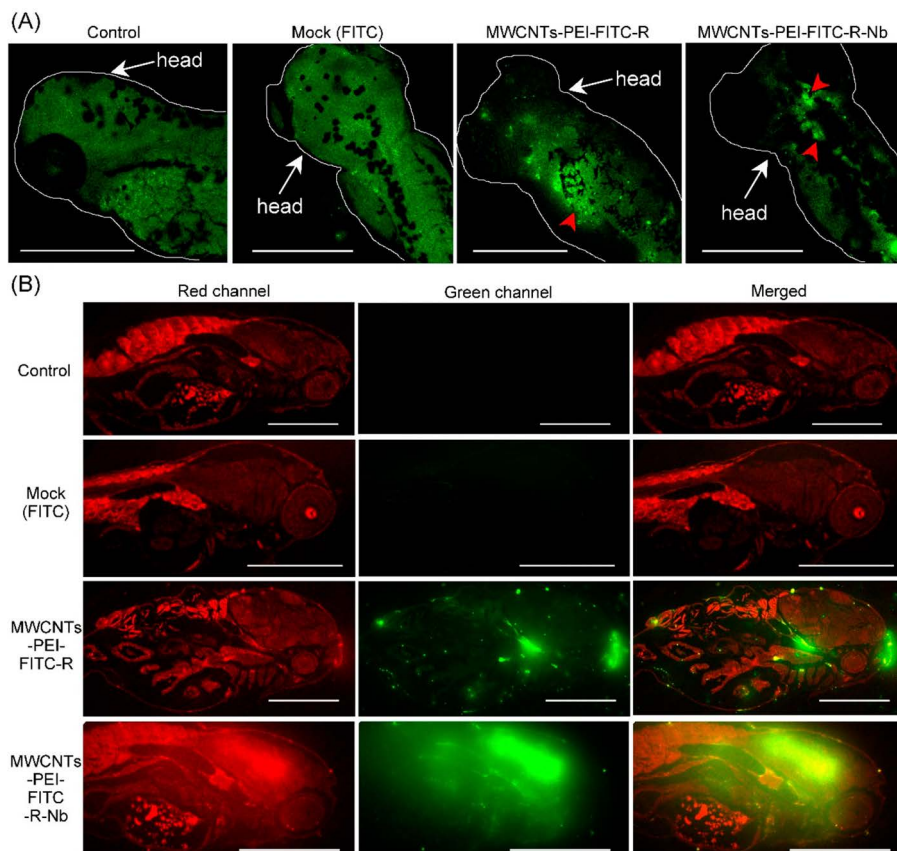


**Figure 1.4** *Panel a:* Zebrafish confocal microscopy figures: control; after incubation with FITC as mock treatment; after incubation with ribavirin-MWCNTs complex; after incubation with ribavirin-Antibody-MWCNTs. *Panel b:* confocal microscopy figures of tissues samples from different groups (control; after incubation with FITC as mock treatment; after incubation with ribavirin-MWCNTs complex; after incubation with ribavirin-Antibody-MWCNTs). Red channel corresponds to indocarbocyanine dye (Dil) fluorescence while the green channel is the FITC fluorescence. Scale bars: 500  $\mu\text{m}$ . Reproduced from ref. 52 with permission from American Chemical Society, Copyright 2019.

loaded, with a supramolecular approach, on oxidized CNTs. The formononetin release gave good results and its effect was evaluated on murine fibroblasts 3T3 and cervical carcinoma HeLa cells as healthy and tumor lines, respectively. While no strong effect was evident in 3T3 treated cells, a cell viability decrease to 40% was reported in the case of HeLa both in the case of the free drug and the formononetin-loaded CNTs. However, the CNT construct was more active in increasing ROS intracellular concentration and in decreasing the mitochondrial membrane potential.<sup>56</sup>

Combretastatin A4 is a compound able to destabilize the tubulin equilibrium, hampering its polymerization and inducing apoptosis but the drawbacks of its use are its aspecificity and low solubility in a biological environment. The conjugation with SWCNTs, through the interposition of glycol chains, allowed a good dispersibility of the construct, that releases 90% of the loaded drug in 50 h. The activity was then evaluated demonstrating much better performances than the free drug.<sup>57</sup>

Metformin is emerging as a new candidate for anticancer drugs, but one of the already clear limitations of its use is the high dosage necessary to exert the activity. With the aim to decrease the quantity of metformin to be administrated, the use of CNTs as a delivery system was explored, employing oxidized CNTs forming salts with the metformin itself. The oxidized CNTs showed a dose-dependent cytotoxicity on HT29R and MCF7. In the case of PC3 the vector showed no toxicity at all. Moreover, due to the presence of the CNTs, the vehiculation of metformin at a concentration of  $2.4 \mu\text{g mL}^{-1}$  induced a reduction of cell viability comparable to that obtained with  $64.5 \mu\text{g mL}^{-1}$  of the free drug, with a very significant increment of activity. Peculiarly, these constructs are scarcely internalized into cells, probably because of the presence of the guanidine unit, which acts as a possible inhibitor of micropinocytosis.<sup>58</sup>

Curcumin as model of an anticancer drug was used to explore the capability of microemulsions of MWCNTs in polymethacrylate to act as drug delivery systems. The authors reported a high content of entrapped curcumin as well as a sustained and prolonged release of the drug at pH 7.4.<sup>59</sup>

To the best of our knowledge, the first report on an oral preparation, specifically tablets, to administrate carbon nanotubes with a drug targeted to the colon was reported in 2019. Oral drug delivery systems targeted to the colon can use different approaches to obtain a selective responsive system, one of those is the enzymatic responsive release adopted in this case. Using wet granulation, the tablets were prepared using MWCNTs and pectin at different percentages. The idea is that peptidase in the colon environment triggers the degradation of pectin with the subsequent release of the entrapped drug. Celecoxib was used as chemoprevention therapy for colorectal cancer. The CNTs presence increased the friability of the tablets but the overall resistance of the preparation was quite good, and the swelling experiments demonstrated that no MWCNTs were released in the solution. The *in vitro* experiments in the presence of peptidases result in a proper degradation of the tablets and the release studies showed a low concentration of the drug in a solution at acidic pH with a substantial release at neutral pH, mimicking the colon.<sup>60</sup>

The delivery of RNA, DNA and their derivatives is also a potential application of MWCNTs.<sup>61</sup> For example, MWCNTs were functionalized with small interfering RNA (siRNA), which is a promising gene silencing compound for directed immunogenetic cancer therapy, in order to stabilize siRNA and deliver it to the targeted cell more efficiently. As *in vivo* delivery of siRNAs to the target cell is limited by the scarce stability, low uptake efficiency and

pharmacokinetics of siRNA, this approach could facilitate the release of the drug or gene into the cell and thus the loaded compound reaches the targeted tissue, escaping lysosomal degradation, enzymatic cleavage and interference of proteins. The result is a greater biostability of nucleic acids with an increase in the ability to reach the target by DNA compared to free DNA. Moreover, Kateb *et al.* suggested that MWCNTs could be used as non-toxic and biodegradable nanocarriers for targeted therapy in brain cancer, a challenging tissue to be reached.<sup>62</sup>

### 1.3 Nanodiamonds

NDs were first produced by a research group from the USSR in July 1963 through the detonation of a 40/60 blend of 2-methyl-1,3,5-trinitrobenzene (TNT) and 1,3,5-trinitroperhydro-1,3,5-triazine (RDX).<sup>63</sup> The first public disclosure of NDs took place with the discovery of 50 Å sized diamonds in meteorites in 1987,<sup>64</sup> and, one year later, the detonation-based production of NDs was reported.<sup>65</sup> Despite the fact that NDs can be produced by different approaches, the most common method is still detonation, being one of the more suitable techniques for large-scale production. In this case, the so-called detonation nanodiamonds present a small primary particle size and a feasible surface functionalization. Another important method of production is milling of diamonds obtained with the high-pressure high temperature process (HPHT),<sup>66</sup> in which presses are used to obtain shock compression of graphite in the presence of metal catalysts. Depending on the chosen catalyst, pressure and temperature vary, usually ranging between 5 and 7 GPa and from 1300 to 1800 °C, respectively. With this process it is possible to obtain particles of irregular shape with a diameter of 10–20 nm, and with a high nitrogen content (100–300 ppm), which confers a very important characteristic to this type of ND. The typical diameter of NDs is in the range of 2 to 100 nm and they are the most stable carbon derivatives with such small dimensions,<sup>67</sup> based on which it is possible to classify NDs into three main groups: nanocrystalline diamond particulates (10–100 nm), ultra-nanocrystalline diamond particulates (0–10 nm, a range that includes detonation nanodiamonds), and diamondoids (~1 to ~2 nm).<sup>68</sup>

NDs are characterized by a core of  $sp^3$  carbon atoms and the possible surface groups are ketone, aldehyde, carboxylic acid, ester, anhydride, cyclic ketone, lactone, amine, epoxide, *etc.*;<sup>69</sup> but in some cases the core can be coated with a graphitic shell composed of  $sp^2$  carbon whose amount is strongly dependent on synthetic methods and purification procedure.<sup>69</sup>

NDs present stability and chemical inertia of the core, high hardness, rigidity, high surface area (20% of the carbon atoms are at the surface),<sup>70</sup> thermal resistivity and conductivity,<sup>71</sup> optical transparency in a wide range of the electromagnetic spectrum, and tendency to aggregate. The optical properties are of particular interest, in particular fluorescence, which was observed especially for HPHT diamonds.<sup>72</sup> This property is due to the presence of

impurities and defects in the lattice, such as vacant nitrogen centers. The centers are able to absorb strongly around 500 nm and to emit at 700 nm. Other advantages are the continuous emission and the photostability.<sup>69,73</sup> Furthermore, since the emission derives from defects inside the reticle, it is not inhibited by surface functionalizations, thus providing an additional advantage in the chemical modifications of this material.

Since cellular uptake can occur through pinocytosis or clathrin-mediated endocytosis, the mode of internalization of the nanoparticles in the cells does not cause any damage to the integrity of the membranes (Figure 1.5).<sup>74</sup> Several factors can play a role in the uptake processes such as the cell type,<sup>75</sup> incubation time, surface characteristics, size, shape and aggregation of the nanodiamonds.<sup>76</sup>

NDs seem to be excellent candidates for biomedical applications, generally showing less cytotoxicity than other nanocarbonaceous materials, such as graphite, graphene and carbon nanotubes.<sup>77</sup> They appear to be well tolerated and show no serious toxic effects *in vivo*.<sup>78</sup> The biocompatibility of NDs has been studied by evaluating both cell death, morphological changes, changes in metabolic activity, alterations in the proliferation and expression of genes and proteins and oxidative stress.<sup>79</sup> The effects of both short-term and long-term nanodiamond treatment have been assessed *in vitro* on different cell cultures, such as macrophages, and several cancer and healthy

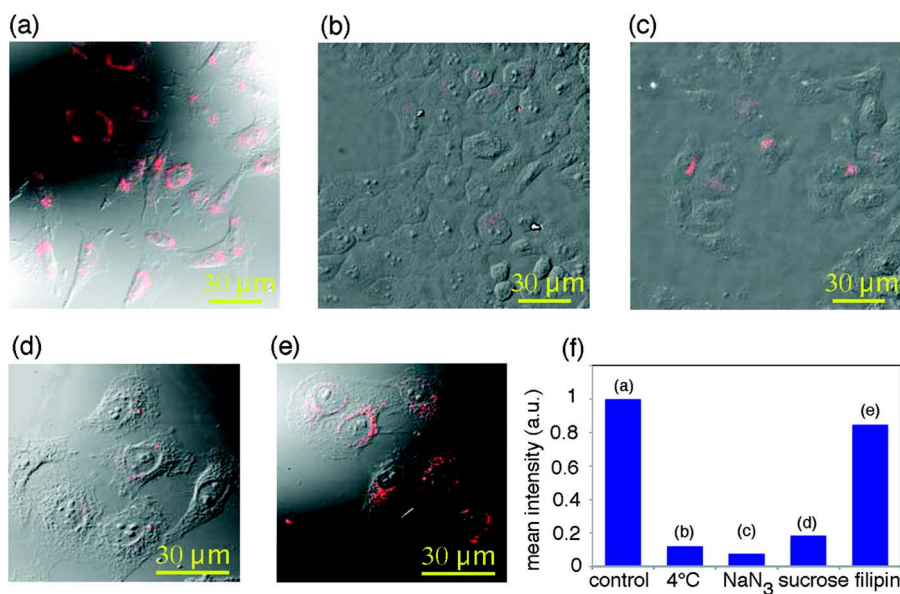


**Figure 1.5** Differential interference contrast (DIC) images of NDs treated HeLa cells at (a) 37 °C; (b) 4 °C; (c) 37 °C in the presence of NaN<sub>3</sub>; (d) 37 °C in the presence of sucrose; (e) 37 °C in the presence of filipin as potential inhibitors of the NDs' cellular uptake. (f) Histogram of mean photoluminescence intensity per cell. Reproduced from ref. 74 with permission, from American Chemical Society, Copyright 2009.

cells. These studies pointed out that NDs are highly biocompatible and highly absorbed inside the cells. Furthermore, these materials do not cause any morphological and metabolic alteration in the cells, they do not affect cell vitality and do not stimulate changes in inflammatory marker levels.<sup>79</sup> *In vivo* tests allowed one to understand that NDs tend to accumulate in lungs, liver, spleen, kidneys and bladder without however altering organ functions. Slight morphological changes in the liver can be observed, but without modification of metabolic activity so as to be considered reversible damage, while some evidence of oxidative stress was found at the lung level.<sup>80</sup> The administration was carried out through different pathways (sub-cutaneous, intravenous, inhalation and oral) and a good tolerability in organisms emerged with no changes in the systemic inflammatory response.<sup>80b</sup>

The evaluation of the possible pro-coagulant effect is important for a possible intravenous administration and the NDs do not seem to alter the prothrombin time, the fibrinogen levels or the platelet count.<sup>81</sup> *In vivo* studies on primates, treated with 15 mg Kg<sup>-1</sup> or 25 mg Kg<sup>-1</sup> of NDs, were performed for six months and the results showed no metabolic alterations, cytotoxicity, inflammatory response or alteration in organ function. Only few alterations of cardiomyocytes, capillaries of the hepatic parenchyma (less pronounced alterations in the group treated with lower dosages) and pulmonary alveoli were detected (Figure 1.6).<sup>81</sup>

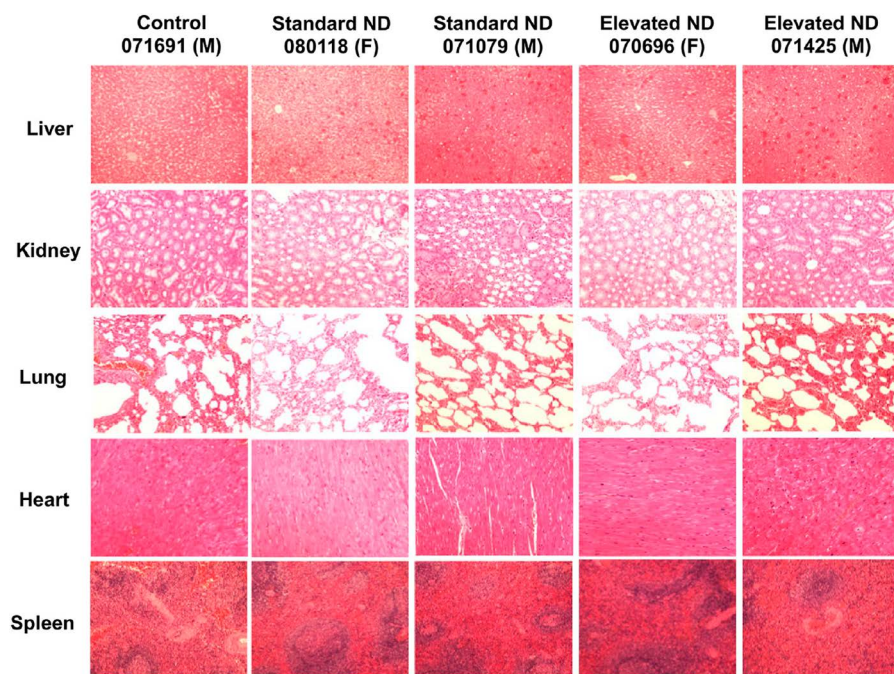


**Figure 1.6** Tissue samples from monkeys treated with different kinds of NDs at 15 or 25 mg kg<sup>-1</sup>, six months after administration. Reproduced from ref. 81 with permission from American Chemical Society, Copyright 2016.

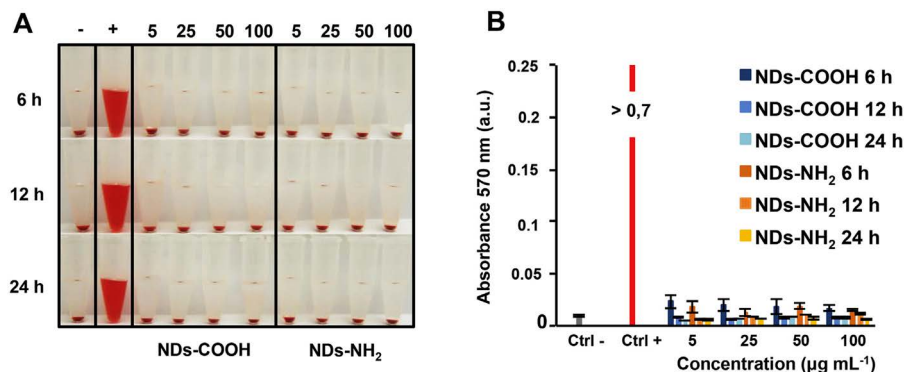


**Figure 1.7** *Panel (A)*. Hemolysis tests at different times and different concentrations of variously functionalized NDs (namely presenting carboxylic or amine groups on the surface). *Panel (B)*. Histogram of the absorbance related to the release of hemoglobin from red blood cells after the ND treatment. Reproduced from ref. 83 with permission from Elsevier, Copyright 2020.

Tsai and collaborators demonstrated the absence of an immune response when NDs were administered by intravenous injection in mice, due to the non-activation of the proinflammatory cytokine TNF- $\alpha$ <sup>82</sup> and recently the absence of hemolytic effect was confirmed (Figure 1.7).<sup>83</sup> In the latter work, the effect of oxidized and amine functionalized nanodiamonds was explored, finding a different behavior of the two materials on the peripheral blood mononuclear cells, with an impact stronger for the one oxidized. Other studies pointed out that oxidized NDs can cause malformations in embryonic cells with a correlation with the concentration and with the presence of carboxylic groups.<sup>78</sup>

### 1.3.1 NDs as Drug Delivery Systems

The application of NDs in drug delivery is one of the most interesting and studied biological applications of these nanoparticles. In fact, they are excellent candidates for drug delivery due to their biocompatibility, dimensional homogeneity and chemical inertia of the core together with a wide variety of functional groups on the surface and large surface area, which allows the adsorption of a considerable amount of molecules. To date, most of the efforts have been devoted to the functionalization of NDs with anticancer drugs using a non-covalent method, in order to leave the drug molecules unaltered.<sup>77</sup> Unfortunately, this approach does not allow one to control the drug release in a proper way. As in the case of CNTs, one of the most studied drugs are anthracyclines.<sup>84</sup> Both in the presence of covalent and non-covalent bonds, these derivatives show an increase in half-life, and decrease in side effects and in drug efflux when delivered using NDs. The chemoresistance

inhibition seems to be related to the cell efflux pumps (ABC, ATP-Binding Cassette) being overcome, with a consequent accumulation of the molecules into the cells.<sup>77</sup> For example, treatment with doxorubicin functionalized nanodiamonds ensured longer retention in 4T1 tumors than the free drug and markedly reduced tumor sizes.<sup>84a</sup> Analogous behavior has been reported in canine kidney cells MDCK, liver cancer LT2-MYC and Huh7 cells and breast cancer cells MDA-MB-231.<sup>85</sup> Wang *et al.* in fact studied the mechanism of action of the NDs-epirubicin complexes, observing that epirubicin is released at acid/neutral pH and, therefore, the release at the blood level is minimal while it is maximized for tumor cells, with a consequent decrease in myelosuppression. This mechanism seems to be related to the internalization into cells by macropinocytosis, considering that macropinosomes merge with lysosomes presenting an acid pH. Once again it has been demonstrated that the retention of the drug into hepatoblastoma LT2-MYC is prolonged compared to the free drug. The efficacy of NDs-Daunorubicin complexes on human erythroleukemia cell line (K562 cells) was also studied, evidencing a constant release of the drug into the cells at pH 4 and the prevention of the drug outflow, with an increase of the drug presence into the cytoplasm.<sup>86</sup>

### 1.3.2 Other Applications of NDs

The so-called nitrogen vacancies (NVs) are defects of the NDs core created within the NDs grid by high energy irradiation (with electrons, protons or helium ions) that induces interruptions in the lattice, while the annealing process (600–800 °C) allows these defects to be filled with nitrogen atoms.<sup>87</sup> These materials emit a red luminescence with a wavelength of about 700 nm if radiated at 560 nm, thus allowing one to trace cellular processes by fluorescence microscopy. NDs containing NV could replace commonly used bioimaging agents due to their longer emission capacity, not being photobleached.<sup>88</sup> HPHT NDs are the most studied as bioimaging agents due to the higher presence of nitrogen in the lattice (300 ppm) in comparison to other kinds of NDs. However, this synthetic method does not produce particles with sizes below 20 nm and this could be an obstacle for biomedical applications. Anyhow, Fu *et al.* used these materials to treat HeLa cells and they observed the translocation of NDs into the cells, with the presence of both aggregates and single particles in the cytoplasm. Since, as already mentioned, the NDs photoluminescence is not influenced by surface modifications, their functionalization is possible without hampering this characteristic as demonstrated with the covalent functionalization of NDs using poly-lysine, which allowed the complexation with DNA by means of electrostatic interactions.<sup>89</sup> This characteristic is very peculiar for these materials and the absence of photobleaching allows the use of NDs in theranostics.

Among the heterogeneous studies of NDs, in one of the early-stage reports, it was demonstrated that the stabilization of protein antigens on the surface of the NDs led to a prolonged and intense immune response, offering the possibility to use NDs in disease prevention.<sup>90</sup>

The incorporation of NDs into polymers, through covalent or non-covalent bonding, can also find application in the biomedical field; for example, NDs functionalized with octadecylamine dispersed in L-poly(lactic acid) allowed an increase in resistance, hardness and Young's modulus of the final material, applicable as a biocompatible and biodegradable/resorbable implantable device in the case of bone damage.<sup>91</sup> NDs are also promising materials in tissue engineering and regenerative medicine. It was shown that they can be an effective neuronal growth platform similar to protein-coated materials when assembled as monolayers.<sup>92</sup>

Wehling *et al.* reported the potential antibacterial activity of NDs and, in particular, of the oxidized ones, able to decrease the viability of *E. coli*, a Gram-negative bacterium, at a concentration of  $5 \text{ mg L}^{-1}$ . NDs presenting a less oxygenated surface did not exert the same effect, suggesting that the mechanism of action is related to the reactivity of these oxygen-containing groups. However, there is a strong influence of the presence of proteins in the environment: the higher the content, the lesser the antibacterial effect (Figure 1.8).<sup>93</sup> This characteristic can be exploited with the use of NDs as excipients in different pharmaceutical formulations. In fact, thanks to their antibacterial properties, they could be used to avoid bacterial contamination.<sup>94</sup> Moreover, thanks to their ability to partially shield UV rays they could be used for the preparation of sun creams and as protective agents with photosensitive drugs<sup>95</sup> and, lastly, they also have a certain antioxidant activity that could be exploited biologically.<sup>80b</sup>

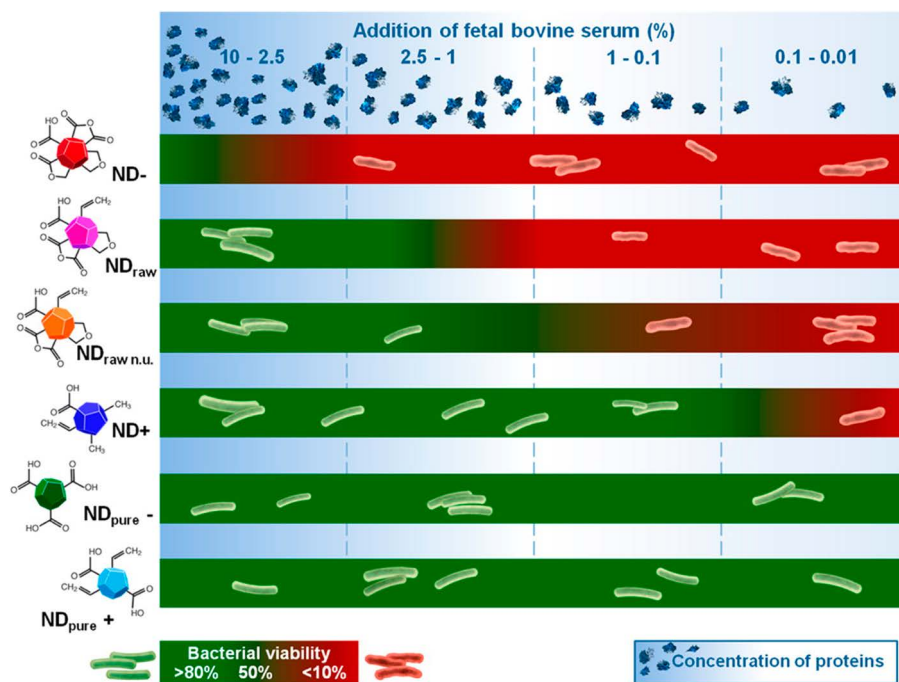


**Figure 1.8** Activity of different NDs vs. bacteria in function of the protein concentration (ranging from 2.5% to 10%) in the used media. Reproduced from ref. 93 with permission from American Chemical Society, Copyright 2014.

## 1.4 Graphene and Carbon Quantum Dots

### 1.4.1 GQDs

Graphene quantum dots (GQDs) basically combine the structure of graphene with the quantum confinement and edge effects of CDs and possess unique properties, which are important for the applications in medicine, electronic, photoluminescence, electrochemical and electrochemiluminescence.<sup>96</sup>

GQDs mostly consist of 1–3 layers of graphene flakes with a diameter of less than 20 nm.<sup>97</sup> The surface groups of GQDs may vary due to the synthetic methodology and the photoluminescence peak may shift depending on the surface functionalization.<sup>98</sup>

Due to the edge effects,<sup>99</sup> the quantum confinement<sup>100</sup> and the unique bulk properties of graphene and the possible functionalization,<sup>101</sup> GQDs have very advantageous properties for a wide range of applications. The synthesis of GQDs may already add different functional groups on the graphene-like surface depending on the chosen preparation. GQDs can be functionalized to adjust biocompatibility, photoluminescence, electronic properties, or optical properties. The intended modifications can be performed with GDQ production using pre-treated starting materials or proper conditions, or as post-production modifications.

The synthesis of nitrogen-doped graphene quantum dots was performed by cutting nitrogen-doped graphene with a hydrothermal method.<sup>102</sup> The so-obtained N-doped GQDs have a N/C atomic ratio of *ca.* 5.6% and diameter of 1–7 nm and show strong blue photoluminescence and upconversion photoluminescence properties. Analogously, fluorinated GQDs, with a F/C atomic ratio of *ca.* 23.7% and diameter of 1–7 nm, can be produced from fluorinated graphene as a modified starting material by using a hydrothermal cutting method.<sup>103</sup> It was shown that fluorination changes the optoelectronic properties of GQDs, upconverts photoluminescence and alters electronic properties similar to the effect of GQD nitrogen doping. The optical properties of solvothermally synthesized GQDs are tunable by the degree of surface oxidation, which brings fine solubility, high stability and upconversion photoluminescence,<sup>98b</sup> and photoluminescence quantum yields can increase from 4.1% to 12.2% with the increase of surface oxidation.

With a simple electrochemical approach, it is possible to produce luminescent and electrocatalytically active nitrogen-doped GQDs with oxygen-rich functional groups from reduced graphene oxide by using tetrabutyl ammonium perchlorate (TBAP) in acetonitrile as electrolyte to introduce N atoms on the surface of GQDs.<sup>98a</sup> The so-produced GQDs present a N/C atomic ratio of *ca.* 4.3%, have blue luminescence and possess electrocatalytic activity.

After the production of GQDs, the usual functionalization is performed through the generation of an amide bond *via* covalent conjugation of amines to the carboxyl groups of graphene quantum dots.<sup>104</sup> Wolk *et al.* activated the carboxylic function with oxalyl chloride treatment, followed by the addition of dodecyl amine. These modified GQDs showed excellent solubility in various organic solvents. Li *et al.* synthesized folic acid functionalized graphene quantum dots loaded with IR780, a lipophilic NIR fluorescent cyanine dye.<sup>105</sup> The preparation took place by mixing folic acid, EDC, NHS

and GQDs in aqueous solution saturated with  $\text{NaHCO}_3$ . Thus, folic acid was covalently attached to the surface of the GQD. The next step was the mixture with IR780 at different concentrations and the latter was linked *via* strong  $\pi$ - $\pi$  stacking interactions. The obtained complex presented improved photostability, enhanced tumor targeting ability and very high photothermal conversion efficiency (87.9%) (Figure 1.9).

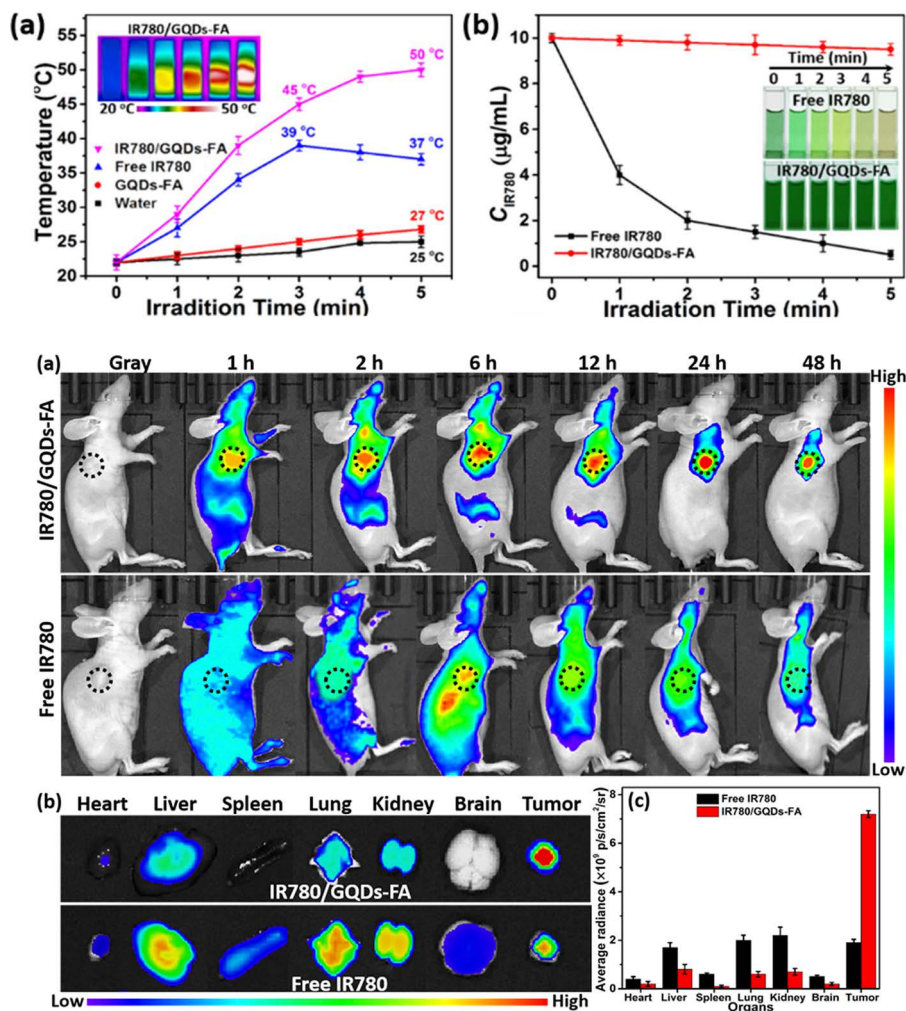


**Figure 1.9** *Top: panel (a).* Photothermal profiles of water, free IR780, GQDs-FA and IR780/GQDs-FA laser irradiated at 808 nm at 1 W cm<sup>-2</sup>. *Panel (b).* Effect of the irradiation time of IR780 and IR780/GQDs-FA on IR780 concentration in aqueous solution. *Bottom: panel (a)* NIR fluorescence intensities of free IR780 and IR780/GQDs-FA in the tumor region. *Panel (b).* *Ex vivo* evaluation of the dissected organs at 24 h post injection. *Panel (c).* Fluorescence intensity of the excised organs after treatment with IR780 and IR780/GQDs-FA. Reproduced from ref. 105 with permission from American Chemical Society, Copyright 2017.

### 1.4.1.1 GQD Applications

GQDs have potential applications in biomedical, optoelectronic, and energy-related fields mainly due to properties such as water solubility and luminescence, which make them excellent candidates for bioimaging and drug delivery.

Kuo *et al.* synthesized GQDs with sizes of approximately 7.1 nm to use them in two-photon photodynamic therapy and simultaneous three-dimensional two-photon bioimaging, especially on multidrug-resistant bacteria. The GQDs were demonstrated to be photosensitizing, with high two-photon absorption in the near IR region, a large absolute cross section of two-photon excitation, strong two-photon luminescence, and impressive two-photon stability. They were coated with two different antibodies, Ab<sub>LPS</sub> and Ab<sub>protein A</sub>, in order to enhance the specificity and efficiency against Gram-negative *E. coli* and Gram-positive MRSA, respectively. The relative maximum at 800 nm was chosen to obtain maximum bactericidal activity. It was shown that GQDs have highly effective photodynamic activity both against Gram-positive and Gram-negative bacteria, due to their capacity to generate reactive oxygen species, which occur with two-photon excitation with ultra-low energy in short photoexcitation time (Figure 1.10).<sup>106</sup>

With the aim of producing novel agents for cancer cell imaging and optical detection of Hg<sup>2+</sup>, Li *et al.* were able to synthesize GQDs with a size range of 2–8 nm from the pyrolysis of maleic acid and folic acid.<sup>107</sup> The resulting folic acid functionalized GQDs display a strong and tunable fluorescence emission under visible light excitation. The authors could tune the fluorescence properties by changing the folic acid ratio in the pyrolysis process. Due

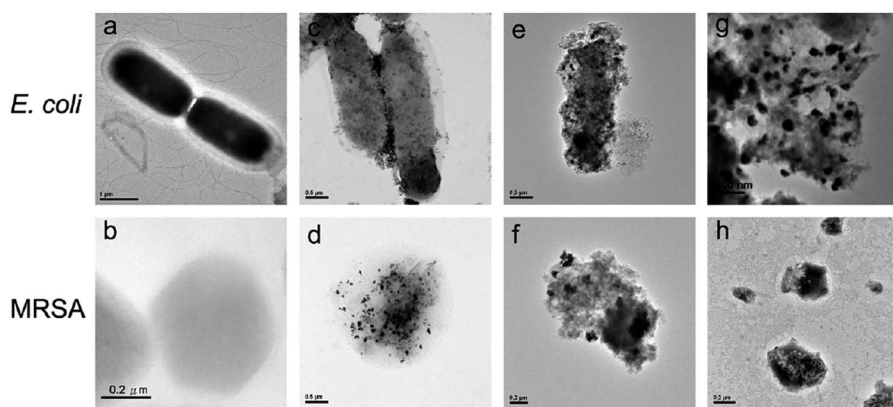


**Figure 1.10** TEM images showing: no treated (a) *E. coli* and (b) MRSA; the effect of the treatment with GQD-Ab<sub>LPS</sub> and GQDs-Ab<sub>protein A</sub> on *E. coli* and MRSA after (c, d) 3 h and (e, f) 5 days of incubation, respectively. (g) Photoexcited GQDs-Ab<sub>LPS</sub> treated *E. coli* and (h) GQDs-Ab<sub>protein A</sub> treated MRSA, respectively, after 3 h of incubation (2.64 mW of TPE for 15 s, excitation at 800 nm, delivered dose OD<sub>600</sub> ~ 0.05 of bacteria and 0.5 μg mL<sup>-1</sup> GQDs). Adapted from ref. 106 with permission from American Chemical Society, Copyright 2016.

to the high number of folic acid units, their good lipid-solubility and their red fluorescence emission, these QDs as turn-on fluorescent probes are more suitable for cancer cell imaging compared with the previously reported graphene quantum dots. The resolution of cell imaging was considerably improved since the red light has better biological tissue penetration and less back spectrum interference compared with blue light. Folic acid functionalized QDs could be easily internalized by the human cervical epithelioid carcinoma cells (HepG2), with an over-expressing folate receptor on the cell membranes. The same study showed that the graphene quantum dots can react with  $\text{Hg}^{2+}$  and therefore a sensitive fluorescence quenching occurs, providing sensitivity and selectivity among all tested metal and nonmetallic ions (Figure 1.11).

### 1.4.2 Carbon Dots

Carbon dots (known as carbon nanodots, C-dots, CDs), one of the newest members of fluorescent carbon nanomaterials,<sup>108</sup> were first reported in 2006 by Sun *et al.*<sup>109</sup> Their shape is described as quasi-spherical, with a diameter below 10 nm. Generally, they have a  $\text{sp}^2$ -conjugated core and present several oxygen-containing species such as carboxyl, hydroxyl and aldehyde groups.<sup>110</sup> In some rare cases, they can contain a diamond-like structure with  $\text{sp}^3$  carbons.<sup>111</sup> They possess excellent water-solubility and the presence of carboxylic functions enable their functionalization with a wide range of organic, polymeric, inorganic, or biological species. The production of carbon dots is achieved by a large variety of simple, fast and cheap synthetic routes. Their photoluminescence, high photostability, and low toxicity make them potential candidates to replace toxic metal-based quantum dots, which pose health concerns and well known environmental and biological hazards.

The structural and physicochemical properties of CDs may remarkably depend on the synthetic routes, which may add various defects, heteroatoms



**Figure 1.11** *Left:* Schematic structure of FA-QDs. *Right:* Bright field (A) and confocal fluorescence microscopy image of HepG2 cells treated with FA-QDs (B) and QDs (insert) at 37 °C for 10 min. Reproduced from ref. 107 with permission from Royal Society of Chemistry.

and functional groups to their structure. Their surface groups contribute to their optical properties and make them water dispersible.<sup>112</sup> Depending on production and purification methodologies, the chemical composition of carbon dots may vary widely. It has been reported that the carbon dots from purified candle soot contain 36.8% carbon, 5.9% hydrogen, 9.6% nitrogen and 44.7% oxygen, and that of raw candle soot contains 91.7% carbon, 1.8% hydrogen, 1.8% nitrogen and 4.4% oxygen.<sup>113</sup> In the same study, solid-state <sup>13</sup>C NMR measurements showed that carbon dots do not have saturated sp<sup>3</sup> carbon atoms and they contain three types of carbon signals: external C=C bonds, internal C=C bonds and C=O bonds.

As GQDs, carbon nanodots also possess tunable photoluminescence properties arising from quantum confinement effects. Their photoluminescence quantum yield is usually lower than GQDs due to the emissive traps on the surface. Therefore, a surface passivation layer is necessary to improve their brightness.

Synthesis and functionalization of carbon dots cannot be separated since most of the surface decorations occur during their production depending on the starting material or solvent. The synthesis of carbon dots can be generally classified into “top-down” and “bottom-up” methods. The process includes cleaving or breaking down of carbonaceous materials *via* chemical, electrochemical, or physical approaches. A variety of small organic molecules can be pyrolyzed or carbonized to obtain carbon nanodots. Top-down approaches are focused on breaking off the bulk carbon material through laser ablation, arc-discharge and electrochemical soaking. In 2006, Sun *et al.* prepared CDs of around 5 nm in diameter *via* laser ablation of a carbon target in the presence of water vapor with argon as the carrier gas.<sup>109</sup> The carbon target was prepared by hot-pressing a mixture of graphite powder and cement, and followed by stepwise baking, curing and annealing in argon flow. The as-produced carbon dots and acid-treated sample have no detectable photoluminescence. However, after surface passivation by attaching PEG<sub>1500N</sub> to the acid-treated carbon structures, bright luminescence emissions were observed. After excitation at 400 nm, the photoluminescence quantum yields ranged from 4% to 10%, supposedly depending on the degree of surface passivation.<sup>109</sup> Hu *et al.* synthesized carbon dots in a one-step procedure, by laser irradiation of a suspension of graphite powders dispersed in organic solvents, achieving at the same time the surface modifications with PEG<sub>200N</sub>. The luminescence was attributed to carboxylate ligands on the surface of carbon dots and the measured quantum yields of the three samples ranged from 3% to 8%. From HR-TEM images it seemed that carbon dots mostly contain defects and the lattice spacing was between 0.20 and 0.23 nm, while the size distribution was 1–8 nm.<sup>111</sup> As already mentioned, in 2007 Liu *et al.* developed a new methodology to synthesize carbon dots from candle soot<sup>113</sup> and the same methodology was studied by Bottini *et al.*<sup>114</sup> The resulting products were purified using polyacrylamide gel electrophoresis (PAGE) to remove relatively big particles, attributed to an incomplete combustion. Oxidative acid treatment was performed to break down inherent interactions and to obtain

well-dispersed carbon dots, which become negatively charged and hydrophilic, due to the introduction of -OH and -COOH groups on their surface. Their diameter was approximately 1 nm and their quantum yields were quite low (<1%), in comparison with those produced through laser ablation.

Sahu *et al.* prepared highly photoluminescent carbon dots in one step from hydrothermal treatment of a renewable bioprecursor, orange juice (*Citrus nobilis deliciosa*). The mechanism for the formation of carbon dots is described as the hydrothermal carbonization of the main constituents of orange juice such as sucrose, glucose, fructose, citric acid and ascorbic acid, at relatively low temperature (120 °C). XPS and FTIR data indicate that the carbon dots are functionalized with hydroxyl, epoxy, carbonyl and carboxylic acid groups and their calculated photoluminescence quantum yield is 26%.<sup>110b</sup> In another study, carbon dots with an average diameter  $3.4 \pm 0.8$  nm were synthesized by Hsu *et al.* from used green tea through grinding, calcination and centrifugation. The obtained carbon dots were highly water-soluble, biocompatible, with photoluminescence at 420 nm when excited at 345 nm (quantum yield 4.3%).<sup>115</sup> In the last few years, a more engineered approach has been proposed, using amino acids and amines as sources for the production of CDs by means of microwaves.<sup>116</sup>

The photoluminescence and optical properties of carbon dots are an intriguing research topic from many aspects. The storage and transport of electrons impacted by light is another attractive research field for carbon dots. Since their discovery, their potential applications in bioimaging, sensing, catalysis, optoelectronics and energy conversion have widely been studied. Cao *et al.*<sup>117</sup> synthesized carbon dots following the procedure reported by Sun *et al.*<sup>109</sup> and passivated their surface with poly-(propionylethylenimine-co-ethylenimine) (PPEI-EI, with EI fraction ~20%). The prepared carbon dots were investigated in MCF-7 cells as a bioimaging agent with two-photon fluorescence microscopy by exciting at 800 nm. It was reported that after 2 h of incubation at 37 °C they emitted strong photoluminescence both on the cell membrane and in the cytoplasm and their internalization was found to be temperature dependent as at 4 °C no cellular uptake was observed.

#### 1.4.2.1 CD Applications

Carbon dots are frequently studied in biological areas because of their low toxicity, good biocompatibility and water solubility. These properties make them good candidates as bioimaging agents and drug nanocarriers.<sup>110b,118</sup> Their *in vitro* cytotoxicity was evaluated by MTT assay on murine fibroblasts L929 and no significant toxicity was reported, indeed they showed to be tolerable at high dose ( $200 \text{ mg mL}^{-1}$ ).<sup>110b</sup> Yang *et al.* evaluated the *in vitro* and *in vivo* toxicity on MCF-7 and HT-29 cell lines of PEG-functionalized carbon dots. They obtained comparable data for PEG-CDs and oligomeric PEG molecules, thus suggesting that these fluorescent dots do not show any toxic effect, like the biocompatible oligomer. Moreover, they do not cause any significant toxic effects on mice at dosages beyond those commonly used for *in vivo* optical imaging.<sup>119</sup> Hsu *et al.* studied the cells growth inhibition of MCF-7,

MDA-MB-231, and HeLa cells, and their bioimaging with carbon dots prepared from calcination of green tea. These materials are effective cell growth inhibitors for MCF-7, MDA-MB-231 and HeLa cells, and cause low toxicity to normal cells such as MCF-10A and LLC-PK1 lines.<sup>115</sup>

Salinas-Castillo *et al.* developed a fluorescent carbon dot nanosensor for selective and sensitive detection of  $\text{Cu}^{2+}$ .<sup>120</sup> The particles had an average size of 12 nm and they were synthesized with a one-step method by pyrolysis of citric acid in the presence of polyethylenimine (PEI) in a microwave oven. The photoluminescence quantum yield was calculated as 30%. The selectivity of the carbon dots for  $\text{Cu}^{2+}$  was studied through the variation of CD fluorescence intensities in the presence of different metal cations. It was observed that fluorescent carbon dots were highly selective for  $\text{Cu}^{2+}$  detection, and  $\text{Fe}^{3+}$  ions caused a quenching effect only when excited at 850 nm, due to the shifting of the maximum emission.

Like the other carbon nanostructures, carbon dots have great potential for bioapplications, especially in drug delivery as they can be tailored to target different tissues, both by using different preparation methods and different surface decorations.

Zhou *et al.* combined and compared three different materials, the so-called black CDs, the gel-like and the yellow carbon dots (respectively, B-CDs, G-CDs and Y-CDs), studying the differences in doxorubicin loading and obtaining a huge increase (>50%) in loading using a combination of CDs. Moreover, these new materials demonstrated their ability to cross the BBB and their affinity for bones in Zebrafish, as in the *in vivo* model.<sup>121</sup> CDs showed efficient uptake in microglial cells as demonstrated by fluorescence measurements of the intrinsic luminescence of QDs. The most interesting findings reported by these authors is the capability of the construct to reduce the secretion of nitric oxide induced by lipopolysaccharide treatment,<sup>122</sup> which can be of utmost interest in neuroprotective approaches.

Another approach to obtain selective affinity for specific tissues, in particular tumor tissues, implied the presence of carboxylic and amino groups on the CDs surface, that allowed the interactions with amino acid transporter 1, with a consequent preferential uptake in human tumor xenografts in mice and in glioma *in vivo* models.<sup>123</sup>

The preparation of the dots using tryptophan as a carbon source has been reported. The choice of the starting material was related to its capability to cross the BBB *via* transporter-mediated endocytosis. In principle, the eventual presence of tryptophan on the CDs' surface after the preparation could allow this material to overcome the BBB, as demonstrated by the presence of dots in the central nervous system in experiments on zebrafish, thus confirming the efficacy of these structures to cross the barrier.<sup>124</sup> A more traditional approach for the selective delivering of molecules into cells by exploiting the overexpression of folate receptors followed decorating CDs with folic acid.<sup>125</sup> In order to obtain structures endowed with selective mitochondrial targeting, some authors proposed triphenylphosphine derivatives in a quite complex construct presenting TPP-D- $\alpha$ -tocopheryl polyethylene glycol succinate derivative linked to the CDs, to form micelle-like structures.<sup>126</sup>

Moreover, the intracellular selectivity was obtained by exploiting a specific decoration of the CDs' surface, as recently reviewed.<sup>127</sup> For example, the Golgi apparatus can be selectively targeted by decorating the CDs' surface with cysteine, thus obtaining the *in situ* image of the apparatus.<sup>128</sup> The introduction of the ricin A-chain also allowed delivery of the latter into the cells escaping the lysosome degradation, due to the presence of CDs (Figure 1.12).<sup>129</sup> Experiments on carcinoma HEP-2 cells enabled the following of different steps of internalizations by colocalizations first with lysosomes, then with Golgi and later on with the endoplasmic reticulum (ER) (Figure 1.12).

A plethora of CDs were prepared starting from different sources, from milk<sup>130</sup> to a combination of citric acid and PEI,<sup>131</sup> but the proper preparation of CDs using chitosan, ethylenediamine and mercaptosuccinic acid leads to materials able to target mitochondria without any further specific functionalization and to be used as markers for these organelles considering their photostability.<sup>132</sup> Analogously, CDs were prepared by hydrothermal treatment of D-glucosamine and *p*-styrenesulfonate to mimic the sulfonate glucosaminoglycane. The so-obtained nanoparticles demonstrated uptake and diffusion into the cellular cytoplasm of rat bone mesenchymal stem cells and promotion of cellular osteogenic and chondrogenic differentiation without influencing the pluripotency of stem cells.<sup>133</sup>

In order to target bone tissue, CDs were prepared using alendronate. The presence of bisphosphonate units on the surface of the dots allowed good interactions with hydroxyapatite when the content of amines on the surface was low. The presence of the CDs was immediately detectable due to their intrinsic fluorescence in *in vivo* experiments on zebrafish.<sup>134</sup> This tropism permits one to envision a future in the treatment of bone diseases for CDs and it was corroborated also by another research in which the dots were decorated with specific peptide sequences able to induce osteoblast adhesion, proliferation and differentiation, and combined with hyperbranched polyurethane. These complexes enhanced osteoconductivity and bone differentiation.<sup>135</sup>

In the frame of drug delivery, antitumor applications are always the major covered topic and CDs are no exception, with a rich literature corpus focused on anthracycline delivery. So far, CDs from many different sources and in varied constructs have been explored. Complex systems have been prepared, as doxorubicin bearing CDs embedded into liposomes,<sup>136</sup> or CDs prepared directly in the presence of amino-functionalized mesoporous silica nanoparticles.<sup>137</sup> The free drug capability to enter into and to kill the cells of three-dimensional multicellular spheroids, used as a tumor model, was outclassed by micelles of CDs loaded with doxorubicin, which proved to be effective also for MCF-7 anthracycline resistant cells.<sup>127</sup>

In order to exploit also the formation of electrostatic bonds between the polyamine units and doxorubicin, carbon dots were coupled to polyamine-containing organosilane derivatives. This construct presented very high drug loading. The cellular uptake in MCF-7 was followed by fluorescence, confirming the presence of the CDs into the cytoplasm. The *in vivo* experiments showed that the efficacy of doxorubicin was higher when associated with CDs than when administered as a free drug.<sup>138</sup>

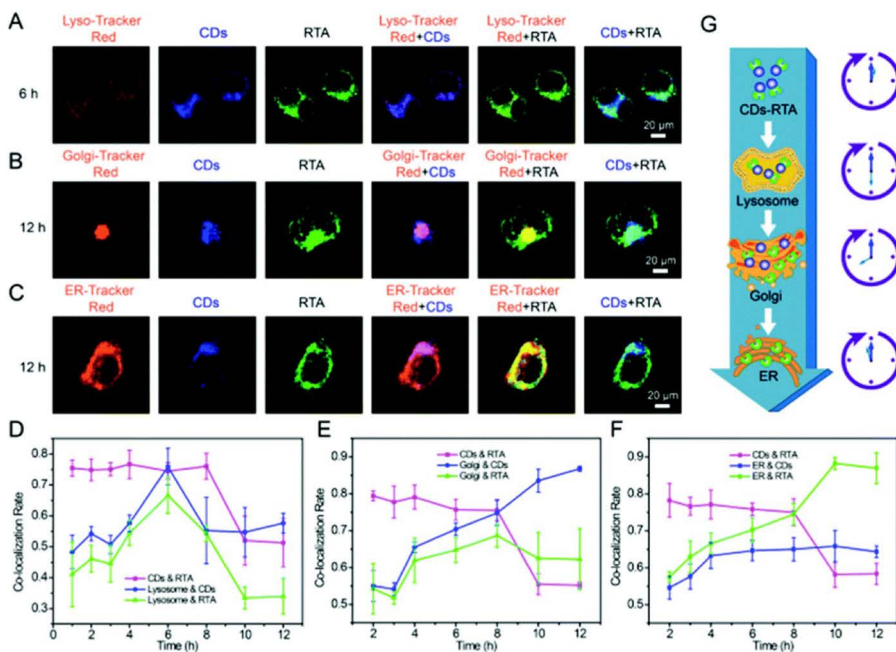
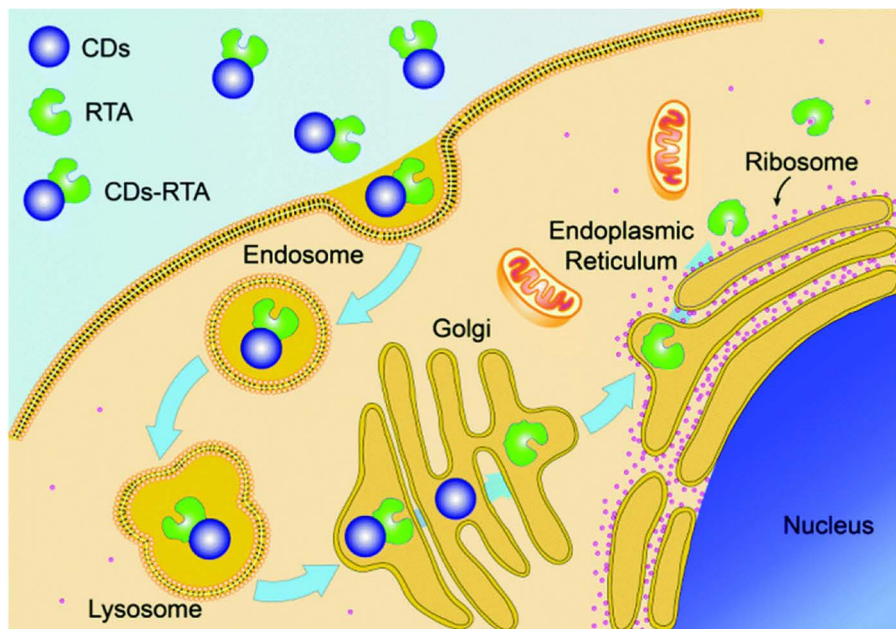


**Figure 1.12** *Left:* Delivery route of the ricin A-chain by Golgi targeting CDs. *Right:* Fluorescence colocalization assay of CDs-RTA conjugates with (A) lysosome, (B) Golgi apparatus and (C) ER after 6 h and 12 h of incubation. Colocalization rate between CDs and RTA with lysosome (D), Golgi apparatus (E) and ER (F), treated with CDs-RTA conjugates at 2, 3, 4, 6, 8, 10 and 12 h. (G) Intracellular transport pathways of CDs-RTA conjugates. Adapted from ref. 129 with permission from Royal Society of Chemistry.

Acid-triggered release of doxorubicin was also achieved using hydrazone linkers<sup>139</sup> or imine-based conjugation of the drug on CDs, with 50% of the release at acidic pH while only 7% was undesirably removed from the vehicle at neutral pH.<sup>140</sup> Also, the carbon dots-mesoporous silica structures loaded with doxorubicin present a pH-sensitive release of the drug but in this case also a thermo-responsive release of the drug upon NIR irradiation was observed.<sup>138</sup> With the same aim, heparin and doxorubicin functionalized carbon dots were prepared obtaining a system responding to acid pH and a better effect than the free drug on cells, while the heparin presence ameliorates hemocompatibility.<sup>141</sup> Good hemocompatibility was also reported for hyaluronic modified CDs used to release doxorubicin.<sup>132</sup> Doxorubicin-conjugated CDs were also able to enter the cellular nuclei and to exert their cytotoxic activity also on cancer stem cells.<sup>142</sup>

CDs decorated with PEG and biotin units at the extremity of the glycolic chains were able to incorporate irinotecan and to release the latter if irradiated in the NIR. The consequent temperature rise not only helps the detachment of the drug but also leads to local hyperthermia, that increases the cell death also in a spheroid tumor model.<sup>143</sup>

Blue- and green-emitting cationic carbon dots were complexed, by means of electrostatic interactions, with  $17\beta$ -estradiol hemisuccinate, able to interact with and be selectively taken up by estrogen receptor-rich cancer cells. In such a way it was possible to stain the responsive cells and to deliver doxorubicin, inducing apoptosis more efficiently than in estrogen receptor negative cells.<sup>144</sup>

The delivery of epirubicin and temozolomide conjugated to CDs on various glioblastoma brain tumor cell lines was achieved by linking transferrin to the CDs at the same time. The complex bearing the targeting agent and the two drugs proved to be very effective also due to the synergistic effect of the two drugs together.<sup>145</sup>

Decoration of carbon dots with a derivatized polyethylenimine provided an amphiphilic construct able to transfer gene and drugs into cells, as demonstrated by Wang *et al.* This material forms micelle structures endowed with a transfection capability higher than Lipofectamine 2000. The encapsulation of apoptosis-inducing siRNA resulted in cell death and the use of the construct in tumor spheroid models corroborates the results.<sup>146</sup> Analogous results of efficient gene knockdown by siRNA delivered by CDs were reported *in vitro* and *in vivo*.<sup>147</sup>

The delivery of inhibitors of miRNAs encoded by various oncogenic viruses is a strategy to avoid the insurgence of related cancers such as Kaposi's sarcoma. Among the silencing agents, locked nucleic acids (LNAs) are very effective antisense molecules and their intracellular delivery by means of CDs leads to the decrease of cell proliferation of KSHV-positive lymphoma cells and to a significant reduction of the tumor size in a primary effusion lymphoma mice model.<sup>148</sup>

These materials were studied also to deliver other drugs. Antibacterial activity of an amoxicillin-CDs preparation was shown and good results were achieved in inhibiting both Gram-positive and Gram-negative bacteria, *S. aureus* and *E. coli*, respectively.<sup>149</sup> Also, the combination with metronidazole

was evaluated against *Porphyromonas gingivalis*, with an efficacy increase of 72% with respect to the free drug.<sup>150</sup> Poly(lactic-co-glycolic acid) combined with CDs provided a good platform for antibiotic release upon irradiation, with a sustained delivery of azithromycin and tobramycin, macrolide and aminoglycoside antibiotics, respectively, with good performances against bacterial biofilm.<sup>151</sup> The combination of bacterial cellulose with titanium dioxide and CDs was demonstrated to be active against *S. aureus*, being at the same time well tolerated by human L929 fibroblast cells, with wound healing effects. These findings suggest the possibility of using such a system for specific bandages, with enhanced cure capability.<sup>152</sup>

Carbon dots deposited on  $\beta$ -cyclodextrin grafted with poly(*N*-vinyl caprolactam) diethylene glycol dimethacrylate copolymer were studied on NIH 3T3 fibroblast cell lines as a thermoresponsive film and no cytotoxicity was found. The local anesthetic lidocaine was loaded on to the film and the *in vitro* and *ex vivo* drug release profiles at body temperatures resulted in a very effective system for transdermal drug administration.<sup>153</sup>

## 1.5 Conclusions

Growing interest in the family of carbon nanostructures has led to the exploration of their potential application in a variety of fields, including which the biomedical area is the most attractive. Currently, the most explored topic is the use of carbon nanostructures as delivery systems, due to features such as their biocompatibility, versatility, capability to load a large number of different chemical structures, and to cross the cell membrane. They seem to be attractive tools for intracellular delivery of drugs, especially anticancer ones, whose toxic effect is non-selective toward cancer cells. Anthracyclines can be mentioned as an example. The selective internalization of carbon nanostructures into tumor cells can be achieved by decorating their surface with molecules recognized by specific transporters or receptors, such as fructose or folic acid and, moreover, the enhanced permeability and retention effect can play an important role in their increased accumulation into cancer tissues.

Certainly, beside conventional anticancer drugs, these materials can be functionalized with nucleic acid derivatives, such as siRNA, and can be used in immunogenic cancer therapy, and many other kinds of molecules, among which we can mention biomolecules with a specific role in tissue regeneration. The previously mentioned decorations, together with the structural consistency of the carbon nanostructures and some other characteristics such as their conductivity, render these materials very attractive in the regenerative medicine.

Nowadays, the peculiar luminescence properties of the newer carbon nanoforms is shifting the focus from CNTs toward NDs, GQDs and CDs. In fact, their intrinsic fluorescence is an excellent base for their use as therapeutic agents, thus combining both therapeutic and diagnostic effects in a single nanoconstruct, without the necessity to introduce fluorescent dyes. Moreover, a number of carbon-based nanostructures proved to efficiently

cross the blood–brain barrier, which is one of the most challenging obstacles in delivering drugs to the central nervous system. In this sense, GQDs and CDs, representing the newest frontier in nanocarbon research, widen the potential application fields. Several properties of these materials, such as biocompatibility, photoluminescence or electronic properties, can be tuned with synthetic or post-synthetic procedures. However, also in this case one of the most explored applications is on their capability to deliver drugs in the treatment of cancer, with the advantage that they allow the application of unconventional therapeutic approaches, such as two-photon photodynamic therapy, affording at the same time cell bioimaging. Promising results concerning the application of fluorescent CDs as theranostic agents have been obtained by several research groups, and many different decorations have been proposed, thus confirming the synthetic and functional versatility of this material that needs to be further explored in the future, especially considering that preparation can start from many different sources (*e.g.* orange juice, tea leaves, tryptophan) and the standardization of their production is still challenging.

## References

1. (a) C. W. Lee, Y. H. Su, Y. C. Chiang, I. T. Lee, S. Y. Li, H. C. Lee, L. F. Hsu, Y. L. Yan, H. Y. Li, M. C. Chen, K. T. Peng and C. H. Lai, *Biomolecules*, 2020, **10**, 514; (b) X. Zhang, Y. Ma, S. Fu and A. Zhang, *Nanomaterials*, 2019, **9**, 1647; (c) A. Munoz, D. Sigwalt, B. M. Illescas, J. Luczkowiak, L. Rodríguez-Pérez, I. Nierengarten, M. Holler, J. S. Remy, K. Buffet, S. P. Vincent, J. Rojo, R. Delgado, J. F. Nierengarten and N. Martín, *Nat. Chem.*, 2016, **8**, 50; (d) B. M. Illescas, J. Rojo, R. Delgado and N. Martín, *J. Am. Chem. Soc.*, 2017, **139**, 6018–6025; (e) J. Ramos-Soriano, J. J. Reina, B. M. Illescas, N. de la Cruz, L. Rodríguez-Pérez, F. Lasala, J. Rojo, R. Delgado and N. Martín, *J. Am. Chem. Soc.*, 2019, **141**, 15403; (f) B. M. Illescas, A. Pérez-Sánchez, A. Mallo, A. Martín-Domenech, I. Rodríguez-Crespo and N. Martín, *J. Mater. Chem. B*, 2020, **8**, 4505–4515; (g) K. Siposova, V. I. Petrenko, O. I. Ivankov, A. Musatov, L. A. Bulavin, M. V. Avdeev and O. A. Kyzyma, *ACS Appl. Mater. Interfaces*, 2020, **12**, 32410–32419.
2. H. Kazemzade and M. Mozafari, *Drug Discovery Today*, 2019, **24**, 898–905.
3. A. A. Shvedova, V. Castranova, E. R. Kisin, D. Schwegler-Berry, A. R. Murray, V. Z. Gandelsman, A. Maynard and P. Baron, *J. Toxicol. Environ. Health, Part A*, 2003, **66**, 1909–1926.
4. A. R. Murray, E. Kisin, S. S. Leonard, S. H. Young, C. Kommineni, V. E. Kagan, V. Castranova and A. A. Shvedova, *Toxicology*, 2009, **257**, 161–171.
5. M. Kaczmarek, O. A. Timofeeva, A. Karaczyn, A. Malyguine, K. S. Kasprzak and K. Salnikow, *Free Radical Biol. Med.*, 2007, **42**, 1246–1257.
6. W. Huang, Y. Wang, G. Luo and F. Wei, *Carbon*, 2003, **41**, 2585–2590.
7. Y. Li, X. Zhang, J. Luo, W. Huang, J. Cheng, Z. Luo, T. Li, F. Liu, G. Xu and X. Ke, *Nanotechnology*, 2004, **15**, 1645–1649.

8. J. Muller, F. Huaux, A. Fonseca, J. B. Nagy, N. Moreau, M. Delos, E. Raymundo-Piñero, F. Béguin, M. Kirsch-Volders, I. Fenoglio, B. Fubini and D. Lison, *Chem. Res. Toxicol.*, 2008, **21**, 1698–1705.
9. V. E. Kagan, N. V. Konduru, W. Feng, B. L. Allen, J. Conroy, Y. Volkov, I. I. Vlasova, N. A. Belikova, N. Yanamala, A. Kapralov, Y. Y. Tyurina, J. Shi, E. R. Kisin, A. R. Murray, J. Franks, D. Stolz, P. Gou, J. Klein-Seetharaman, B. Fadeel, A. Star and A. A. Shvedova, *Nat. Nanotechnol.*, 2010, **5**, 354–359.
10. C. M. Sayes, F. Liang, J. L. Hudson, J. Mendez, W. Guo, J. M. Beach, V. C. Moore, C. D. Doyle, J. L. West, W. E. Billups, K. D. Ausman and V. L. Colvin, *Toxicol. Lett.*, 2006, **161**, 135–142.
11. H. Dumortier, S. Lacotte, G. Pastorin, R. Marega, W. Wu, D. Bonifazi, J.-P. Briand, M. Prato, S. Muller and A. Bianco, *Nano Lett.*, 2006, **6**, 1522–1528.
12. D. B. Warheit, B. R. Laurence, K. L. Reed, D. H. Roach, G. A. M. Reynolds and T. R. Webb, *Toxicol. Sci.*, 2004, **77**, 117–125.
13. D. Dutta, S. K. Sundaram, J. G. Teeguarden, B. J. Riley, L. S. Fifield, J. M. Jacobs, S. R. Addleman, G. A. Kaysen, B. M. Moudgil and T. J. Weber, *Toxicol. Sci.*, 2007, **100**, 303–315.
14. C. A. Poland, R. Duffin, I. Kinloch, A. Maynard, W. A. H. Wallace, A. Seaton, V. Stone, S. Brown, W. MacNee and K. Donaldson, *Nat. Nanotechnol.*, 2008, **3**, 423–428.
15. K. Kostarelos, *Nat. Biotechnol.*, 2008, **26**, 774–776.
16. S.-T. Yang, J. Luo, Q. Zhou and H. Wang, *Theranostics*, 2012, **2**, 271.
17. L. Lacerda, M. A. Herrero, K. Venner, A. Bianco, M. Prato and K. Kostarelos, *Small*, 2008, **4**, 1130–1132.
18. R. MacDonald, B. Laurenzi, G. V. P. Ajayan and J. Stegemann, *J. Biomed. Mater. Res.*, 2005, **74**, 489–496.
19. A. Galano, *J. Phys. Chem. C*, 2008, **112**, 8922–8927.
20. (a) M. M. Elsayed, M. E. Mostafa, E. Alaaeldin, H. Sarhan, M. Shaykoon, S. Allam, A. Ahmed and B. Elsadek, *Int. J. Nanomed.*, 2019, **14**, 8445; (b) C. Falank, A. W. Tasset, M. Farrell, S. Harris, P. Everill, M. Marinkovic and M. R. Reagan, *Nanomed. Nanotechnol.*, 2019, **20**, 102025.
21. T. Saliev, *CJ. Carbon Res.*, 2019, **5**, 29.
22. Y.-J. Lu, K.-C. Wei, C.-C. M. Ma, S.-Y. Yang and J.-P. Chen, *Colloids Surf., B*, 2012, **89**, 1–9.
23. (a) N. W. S. Kam, Z. Liu and H. Dai, *Angew. Chem., Int. Ed.*, 2006, **45**, 577–581; (b) K. Kostarelos, L. Lacerda, G. Pastorin, W. Wu, S. Wieckowski, J. Luangsivilay, S. Godefroy, D. Pantarotto, J.-P. Briand, S. Muller, M. Prato and A. Bianco, *Nat. Nanotechnol.*, 2007, **2**, 108–113.
24. H. A. F. M. Hassan, S. S. Diebold, L. A. Smyth, A. A. Walters, G. Lombardi and K. T. Al-Jamal, *J. Controlled Release*, 2019, **297**, 79–90.
25. L. Lacerda, J. Russier, G. Pastorin, M. A. Herrero, E. Venturelli, H. Dumortier, K. T. Al-Jamal, M. Prato, K. Kostarelos and A. Bianco, *Biomaterials*, 2012, **33**, 3334–3343.
26. N. Saito, Y. Usui, K. Aoki, N. Narita, M. Shimizu, K. Hara, N. Ogiwara, K. Nakamura, N. Ishigaki, H. Kato, S. Taruta and M. M. Endo, *Chem. Soc. Rev.*, 2009, **38**, 1897–1903.

27. (a) J. Meng, L. Song, J. Meng, H. Kong, G. Zhu, C. Wang, L. Xu, S. Xie and H. Xu, *J. Biomed. Mater. Res., Part A*, 2006, **79A**, 298–306; (b) A. O. Lobo, M. A. F. Corat, E. F. Antunes, M. B. S. Palma, C. Pacheco-Soares, E. E. Garcia and E. J. Corat, *Carbon*, 2010, **48**, 245–254.
28. G. Cellot, E. Cilia, S. Cipollone, V. Rancic, A. Sucapane, S. Giordani, L. Gambazzi, H. Markram, M. Grandolfo, D. Scaini, F. Gelain, L. Casalis, M. Prato, M. Giugliano and L. Ballerini, *Nat. Nanotechnol.*, 2009, **4**, 126–133.
29. T.-I. Chao, S. Xiang, J. F. Lipstate, C. Wang and J. Lu, *J. Adv. Mater.*, 2010, **22**, 3542–3547.
30. E. B. Malarkey, R. C. Reyes, B. Zhao, R. C. Haddon and V. Parpura, *Nano Lett.*, 2009, **9**, 264–268.
31. X. Zhang, S. Prasad, S. Niyogi, A. Morgan, M. Ozkan and C. S. Ozkan, *Sens. Actuators, B*, 2005, **106**, 843–850.
32. D. Rugar, H. J. Mamin, M. H. Sherwood, M. Kim, C. T. Rettner, K. Ohno and D. D. Awschalom, *Nat. Nanotechnol.*, 2015, **10**, 120–124.
33. J. A. Roman, T. L. Niedzielko, R. C. Haddon, V. Parpura and C. L. Floyd, *J. Neurotrauma*, 2011, **28**, 2349–2362.
34. B. Chen, H. Zhang, C. Zhai, N. Du, C. Sun, J. Xue, D. Yang, H. Huang, B. Zhang and Q. J. Xie, *Mater. Chem.*, 2010, **20**, 9895–9902.
35. O. Vittorio, S. L. Duce, A. Pietrabissa and A. Cuschieri, *Nanotechnology*, 2011, **22**, 095706.
36. A. Al Faraj, K. Cieslar, G. Lacroix, S. Gaillard, E. Canet-Soulas and Y. Crémillieux, *Nano Lett.*, 2009, **9**, 1023–1027.
37. S. Y. Hong, G. Tobias, K. T. Al-Jamal, B. Ballesteros, H. Ali-Boucetta, S. Lozano-Perez, P. D. Nellist, R. B. Sim, C. Finucane, S. J. Mather, M. L. H. Green, K. Kostarelos and B. G. Davis, *Nat. Mater.*, 2010, **9**, 485–490.
38. (a) J. T.-W. Wang, C. Spinato, R. Klippstein, P. M. Costa, M. Martincic, E. Pach, A. Perez Ruiz de Garibay, C. Ménard-Moyon, R. Feldman, Y. Michel, M. Šefl, I. Kyriakou, D. Emfietzoglou, J.-C. Saccavini, B. Ballesteros, G. Tobias, A. Bianco and K. T. Al-Jamal, *Carbon*, 2020, **162**, 410–422; (b) J. T.-W. Wang, R. Klippstein, M. Martincic, E. Pach, R. Feldman, M. Šefl, Y. Michel, D. Asker, J. K. Sosabowski, M. Kalbac, T. Da Ros, C. Ménard-Moyon, A. Bianco, I. Kyriakou, D. Emfietzoglou, J.-C. Saccavini, B. Ballesteros, K. T. Al-Jamal and G. Tobias, *ACS Nano*, 2020, **14**, 129–141.
39. C. Fabbro, H. Ali-Boucetta, T. Da Ros, K. Kostarelos, A. Bianco and M. Prato, *Chem. Commun.*, 2012, **48**, 3911–3926.
40. P. S. O. Ozgen, S. Atasoy, B. Z. Kurt, Z. Durmus, G. Yigite and A. Dag, *J. Mater. Chem. B*, 2020, **8**, 3123.
41. A. Gangrade and B. B. Mandal, *ACS Biomater. Sci. Eng.*, 2019, **5**, 2365–2381.
42. H. V. Grushevskaya and N. G. Krylova, *Curr. Pharm. Des.*, 2018, **24**, 5207–5218.
43. N. Badea, M. M. Craciun, A. S. Dragomir, M. Balas, A. Dinischiotu, C. Nistor, C. Gavan and D. Ionita, *Mater. Chem. Phys.*, 2020, **241**, 122435.

44. W. Yi, P. Zhang, J. Hou, W. Chen, L. Bai, S. Yoo, A. Khalid and X. Hou, *Int. J. Biol. Macromol.*, 2018, **120**, 1525–1532.
45. S. Pasban, H. Raissi, M. Pakdel and F. Farzad, *Int. J. Pharm.*, 2019, **568**, 118491.
46. H. Moradnia, H. Raissi and A. Bakhtiari, *J. Biomol. Struct. Dyn.*, 2019, **37**(10), 2477–2486.
47. S. K. Prajapati, A. Jain, C. Shrivastava and A. K. Jain, *Int. J. Biol. Macromol.*, 2019, **123**, 691–703.
48. P. Zhang, W. Yi, J. Hou, S. Yoo, W. Jin and Q. Yang, *Int. J. Nanomed.*, 2018, **13**, 3069–3080.
49. A. Al Faraj, A. S. Shaik, E. Ratemi and R. Halwani, *J. Controlled Release*, 2016, **225**, 240–251.
50. M. R. Berber, H. Elkhenany, I. H. Hafez, A. El-Badawy, M. Essawy and N. El-Badri, *Nanomedicine*, 2020, **15**, 793–808.
51. Y. You, N. Wang, L. He, C. Shi, D. Zhang, Y. Liu, L. Luo and T. Chen, *Dalton Trans.*, 2019, **48**, 1569–1573.
52. S. Zhu, A.-G. Huang, F. Luo, J. Li, J. Li, L. Zhu, L. Zhao, B. Zhu, F. Ling and G.-X. Wang, *ACS Appl. Mater. Interfaces*, 2019, **11**, 19006–19016.
53. N. Dlamini, H. E. Mukaya, R. L. Van Zyl, C. T. Chen, R. J. Zeevaart and X. Y. Mbianda, *Mater. Sci. Eng., C*, 2019, **104**, 109967.
54. P. J. Harsha, N. Thotakura, M. Kumar, S. Sharma, A. Mittal, R. K. Khurana, B. Singh, P. Negi and K. Raza, *J. Drug Delivery Sci. Technol.*, 2019, **53**, 101186.
55. K.-C. Tay, L. T.-H. Tan, C. K. Chan, S. L. Hong, K.-G. Chan, W. H. Yap, P. Pusparajah, L.-H. Lee and B.-H. Goh, *Front. Pharmacol.*, 2019, **10**, 820.
56. B. Guo, C. Liao, X. Liu and J. Yi, *Drug Des., Dev. Ther.*, 2018, **12**, 2815–2826.
57. M. Assali, A. N. Zaid, N. Kittana, D. Hamad and J. Amer, *Nanotechnology*, 2018, **29**, 245101.
58. G. Biagiotti, M. C. Ligi, S. Fedeli, E. Pranzini, T. Gamberi, S. Cicchi and P. Paoli, *J. Drug Delivery Sci. Technol.*, 2018, **47**, 254–258.
59. R. A. Sobh, H. E. Nasr, A. B. Moustafa and W. S. Mohamed, *J. Pharm. Invest.*, 2019, **49**, 45–55.
60. W. Zhu, C. Han, Y. Dong and B. Jian, *J. Radioanal. Nucl. Chem.*, 2019, **320**, 503–512.
61. M. A. Herrero, F. M. Toma, K. T. Al-Jamal, K. Kostarelos, A. Bianco, T. Da Ros, F. Bano, L. Casalis, G. Scoles and M. Prato, *J. Am. Chem. Soc.*, 2009, **131**(28), 9843–9848.
62. B. Kateb, M. Van Handel, L. Zhang, M. J. Bronikowski, H. Manohara and B. Badie, *NeuroImage*, 2007, **37**, S9–S17.
63. V. V. Danilenko, *Phys. Solid State*, 2004, **46**, 595.
64. R. S. Lewis, T. Ming, J. E. Wacker, E. Anders and E. Steel, *Nature*, 1987, **326**, 160.
65. (a) A. Lyamkin, E. Petrov, A. Ershov, G. Sakovich, A. Staver and V. Titov, *Dokl. Akad. Nauk SSSR*, 1988, **302**, 611; (b) N. R. Greiner, D. S. Phillips, J. D. Johnson and F. Volk, *Nature*, 1988, **333**, 440.
66. F. P. Bundy, H. T. Hall, H. M. Strong and R. H. Wentorf, *Nature*, 1955, **176**, 51.

67. I. I. Kulakova, *Phys. Solid State*, 2004, **46**, 636.
68. A. M. Schrand, S. A. Hens and O. A. Shenderova, *Crit. Rev. Solid State*, 2009, **34**, 18.
69. V. M. Mochalin, O. Shenderova, D. Ho and Y. Gogotsi, *Nat. Nanotechnol.*, 2012, **7**, 11.
70. S. Osswald, G. Yushin, V. Mochalin, S. O. Kucheyev and Y. Gogotsi, *J. Am. Chem. Soc.*, 2006, **128**, 11635.
71. (a) A. Krueger, *Adv. Mater.*, 2008, **20**, 2445; (b) Y. Liu, Z. Gu, J. L. Margrave and V. N. Khabashesku, *Chem. Mater.*, 2004, **16**, 3924; (c) V. N. Mochalin and Y. Gogotsi, *Diamond Relat. Mater.*, 2015, **58**, 161.
72. E. A. Ekimov and M. V. Kondrin, *Semicond. Semimetals*, 2020, **103**, 161–199.
73. A. Krueger, *J. Mater. Chem.*, 2011, **21**, 12571.
74. O. Faklaris, V. Joshi, T. Irinopoulou, P. Tauc, M. Sennour, H. Girard, C. Gesset, J. C. Arnault, A. Thorel, J. P. Boudou, P. A. Curmi and F. Tressart, *ACS Nano*, 2009, **3**, 3955–3962.
75. C. Gaillard, H. A. Girard, C. Falck, V. Paget, V. Simic, N. Ugolin, P. Bergonzo, S. Chevillard and J. C. Arnault, *RSC Adv.*, 2014, **4**, 3566–3572.
76. R. Kaur and I. Badea, *Int. J. Nanomed.*, 2013, **8**, 203–220.
77. D. G. Lim, R. E. Prim, K. H. Kim, E. Kang, K. Park and S. H. Jeong, *Int. J. Pharm.*, 2016, **514**, 41–51.
78. K. J. van der Laan, M. Hasani, T. Zheng and R. Schirhagl, *Small*, 2018, **14**, 1704263.
79. M. Chipaux, K. J. van der Laan, S. R. Hemelaar, M. Hasani, T. Zheng and R. Schirhagl, *Small*, 2018, **14**, 1704263.
80. (a) L. Moore, V. Grobárová, H. Shen, H. B. Man, J. Míčová, M. Ledvina, J. Štursa, M. Nesladek, A. Fišerová and D. Ho, *Nanoscale*, 2014, **6**, 11712–11721; (b) K. J. van der Laan, M. Hasani, T. Zheng and R. Schirhagl, *Small*, 2018, **14**, 1703838.
81. L. Moore, J. Yang, T. T. Ha Lan, E. Osawa, D. K. Lee, W. D. Johnson, J. Xi, E. K. H. Chow and D. Ho, *ACS Nano*, 2016, **10**, 7385–7400.
82. L. W. Tsai, Y. C. Lin, E. Perevedentseva, A. Lugovtsov, A. Priezzhev and C. L. Cheng, *Int. J. Mol. Sci.*, 2016, **17**, 1111.
83. L. Fusco, E. Avitabile, V. Armuzza, M. Orecchioni, A. Istif, D. Bedognetti, T. Da Ros and L. G. Delogu, *Carbon*, 2020, **160**, 390–404.
84. (a) E. K. Chow, X.-Q. Zhang, M. Chen, R. Lam, E. Robinson, H. Huang, D. Schaffer, E. Osawa, A. Goga and D. Ho, *Sci. Transl. Med.*, 2011, **3**, 73ra21; (b) H. B. Man, H. Kim, H.-J. Kim, E. Robinson, W. K. Liu, E. K.-H. Chow and D. Ho, *Nanomed. Nanotechnol.*, 2014, **10**, 359–369; (c) J. Xiao, X. Duan, Q. Yin, Z. Zhang, H. Yu and Y. Li, *Biomaterials*, 2013, **34**, 9648–9656.
85. X. Wang, X. C. Low, W. Hou, L. N. Abdullah, T. B. Toh, M. M. A. Rashid, D. Ho and E. K. H. Chow, *ACS Nano*, 2014, **8**, 12151–12166.
86. H. B. Man, H. Kim, H. J. Kim, E. Robinson, W. K. Liu, E. K. H. Chow and D. Ho, *Nanomedicine*, 2014, **10**, 359–369.
87. R. Kaur and I. Badea, *Int. J. Nanomed.*, 2013, **8**, 203–220.

88. C. C. Fu, H. Y. Lee, K. Chen, T. S. Lim, H. Y. Wu, P. K. Lin, P. K. Wei, P. H. Tsao, H. C. Chang and W. Fann, *Proc. Natl. Acad. Sci. U. S. A.*, 2007, **104**, 727–732.
89. C. C. Fu, H. Y. Lee, K. Chen, T. S. Lim, H. Y. Wu, P. K. Lin, P. K. Wei, P. H. Tsao, H. C. Chang and W. Fann, *Proc. Natl. Acad. Sci. U. S. A.*, 2007, **104**, 727–732.
90. N. Kossovsky, A. Gelman, H. J. Hnatyszyn, S. Rajguru, R. L. Garrell, S. Torbati, S. S. F. Freitas and G. M. Chows, *Bioconjugate Chem.*, 1995, **6**, 507–511.
91. Q. Zhang, V. N. Mochalin, I. Neitzel, I. Y. Knoke, J. Han, C. A. Klug, J. G. Zhou, P. I. Lelkes and Y. Gogotsi, *Biomater*, 2011, **32**, 87–94.
92. A. Thalhammer, R. J. Edgington, L. A. Cingolani, R. Schoepfer and R. B. Jackman, *Biomaterials*, 2010, **31**, 2097–2104.
93. J. Wehling, R. Dringen, R. N. Zare, M. Maas and K. Rezwani, *ACS Nano*, 2014, **8**, 6475–6483.
94. A. Chatterjee, E. Perevedentseva, M. Jani, C. Y. Cheng, Y. S. Ye, P. H. Chung and C. L. Cheng, *J. Biomed. Opt.*, 2015, **20**, 0510141.
95. O. Shenderova, V. Grichko, S. Hens and J. Walch, *Diamond Relat. Mater.*, 2007, **16**, 2003–2008.
96. (a) H. Sun, L. Wu, W. Wei and X. Qu, *Mater. Today*, 2013, **16**, 433–442; (b) S. Zhou, H. Xu, W. Gan and Q. Yuan, *RSC Adv.*, 2016, **6**, 110775–110788; (c) J. Ge, M. Lan, B. Zhou, W. Liu, L. Guo, H. Wang, Q. Jia, G. Niu, X. Huang, H. Zhou, X. Meng, P. Wang, C.-S. Lee, W. Zhang and X. Han, *Nat. Commun.*, 2014, **5**, 4596; (d) J. Shen, Y. Zhu, X. Yang and C. Li, *Chem. Commun.*, 2012, **48**, 3686–3699.
97. (a) D. Pan, J. Zhang, Z. Li and M. Wu, *Adv. Mater.*, 2010, **22**, 734–738; (b) J. Peng, W. Gao, B. K. Gupta, Z. Liu, R. Romero-Aburto, L. Ge, L. Song, L. B. Alemany, X. Zhan, G. Gao, S. A. Vithayathil, B. A. Kaiparettu, A. A. Marti, T. Hayashi, J. J. Zhu and P. M. Ajayan, *Nano Lett.*, 2012, **12**, 844–849; (c) Y. Li, Y. Hu, Y. Zhao, G. Shi, L. Deng, Y. Hou and L. Qu, *Adv. Mater.*, 2011, **23**, 776–780.
98. (a) Y. Li, Y. Zhao, H. Cheng, Y. Hu, G. Shi, L. Dai and L. Qu, *J. Am. Chem. Soc.*, 2012, **134**, 15–18; (b) S. Zhu, J. Zhang, X. Liu, B. Li, X. Wang, S. Tang, Q. Meng, Y. Li, C. Shi, R. Hu and B. Yang, *RSC Adv.*, 2012, **2**, 2717–2720; (c) Y. Dong, J. Shao, C. Chen, H. Li, R. Wang, Y. Chi, X. Lin and G. Chen, *Carbon*, 2012, **50**, 4738–4743.
99. L. Kittiratanawasin and S. Hannongbua, *Integr. Ferroelectr.*, 2016, **175**, 211–219.
100. L. A. Ponomarenko, F. Schedin, M. I. Katsnelson, R. Yang, E. W. Hill, K. S. Novoselov and A. K. Geim, *Science*, 2008, **320**, 356–358.
101. S. Zhu, J. Zhang, C. Qiao, S. Tang, Y. Li, W. Yuan, B. Li, L. Tian, F. Liu, R. Hu, H. Gao, H. Wei, H. Zhang, H. Sun and B. Yang, *Chem. Commun.*, 2011, **47**, 6858–6860.
102. M. Li, W. Wu, W. Ren, H.-M. Cheng, N. Tang, W. Zhong and Y. Du, *Appl. Phys. Lett.*, 2012, **101**, 103107.

103. Q. Feng, Q. Cao, M. Li, F. Liu, N. Tang and Y. Du, *Appl. Phys. Lett.*, 2013, **102**, 013111.
104. A. Wolk, M. Rosenthal, S. Neuhaus, K. Huber, K. Brassat, J. K. N. Lindner, R. Grothe, G. Grundmeier, W. Bremser and R. Wilhelm, *Sci. Rep.*, 2018, **8**, 5843.
105. S. Li, S. Zhou, Y. Li, X. Li, J. Zhu, L. Fan and S. Yang, *ACS Appl. Mater. Interfaces*, 2017, **9**, 22332–22341.
106. W.-S. Kuo, C.-Y. Chang, H.-H. Chen, C.-L. L. Hsu, J.-Y. Wang, H.-F. Kao, L. C.-S. Chou, Y.-C. Chen, S.-J. Chen, W.-T. Chang, S.-W. Tseng, P.-C. Wu and Y.-C. Pu, *ACS Appl. Mater. Interfaces*, 2016, **8**, 30467–30474.
107. R. Li, X. Wang, Z. Li, H. Zhu and J. Liu, *New J. Chem.*, 2018, **42**, 4352–4360.
108. F. Arcudi, L. Đorđević and M. Prato, *Acc. Chem. Res.*, 2019, **52**, 2070–2079.
109. Y.-P. Sun, B. Zhou, Y. Lin, W. Wang, K. A. S. Fernando, P. Pathak, M. J. Meziani, B. A. Harruff, X. Wang, H. Wang, P. G. Luo, H. Yang, M. E. Kose, B. Chen, L. M. Veca and S.-Y. Xie, *J. Am. Chem. Soc.*, 2006, **128**, 7756–7757.
110. (a) S. C. Ray, A. Saha, N. R. Jana and R. Sarkar, *J. Phys. Chem. C*, 2009, **113**, 18546–18551; (b) S. Sahu, B. Behera, T. K. Maiti and S. Mohapatra, *Chem. Commun.*, 2012, **48**, 8835–8837.
111. S.-L. Hu, K.-Y. Niu, J. Sun, J. Yang, N.-Q. Zhao and X.-W. Du, *J. Mater. Chem.*, 2009, **19**, 484–488.
112. L. Wang, S.-J. Zhu, H.-Y. Wang, S.-N. Qu, Y.-L. Zhang, J.-H. Zhang, Q.-D. Chen, H.-L. Xu, W. Han, B. Yang and H.-B. Sun, *ACS Nano*, 2014, **8**, 2541–2547.
113. H. Liu, T. Ye and C. Mao, *Angew. Chem.*, 2007, **119**, 6593–6595.
114. M. Bottini and T. Mustelin, *Nat. Nanotechnol.*, 2007, **2**, 599.
115. P.-C. Hsu, P.-C. Chen, C.-M. Ou, H.-Y. Chang and H.-T. Chang, *J. Mater. Chem. B*, 2013, **1**, 1774–1781.
116. (a) F. Arcudi, L. Đorđević and M. Prato, *Angew. Chem.*, 2016, **128**, 2147–2152; (b) F. Arcudi, L. Đorđević and M. Prato, *Angew. Chem., Int. Ed.*, 2017, **56**, 4170–4173.
117. L. Cao, X. Wang, M. J. Meziani, F. Lu, H. Wang, P. G. Luo, Y. Lin, B. A. Harruff, L. M. Veca, D. Murray, S.-Y. Xie and Y.-P. Sun, *J. Am. Chem. Soc.*, 2007, **129**, 11318–11319.
118. (a) B. Kong, A. Zhu, C. Ding, X. Zhao, B. Li and Y. Tian, *Adv. Mater.*, 2012, **24**, 5844–5848; (b) Q. Wang, X. Huang, Y. Long, X. Wang, H. Zhang, R. Zhu, L. Liang, P. Teng and H. Zheng, *Carbon*, 2013, **59**, 192–199; (c) Q. Li, T. Y. Ohulchanskyy, R. Liu, K. Koynov, D. Wu, A. Best, R. Kumar, A. Bonoiu and P. N. Prasad, *J. Phys. Chem. C*, 2010, **114**, 12062–12068.
119. S.-T. Yang, X. Wang, H. Wang, F. Lu, P. G. Luo, L. Cao, M. J. Meziani, J.-H. Liu, Y. Liu, M. Chen, Y. Huang and Y.-P. Sun, *J. Phys. Chem. C*, 2009, **113**, 18110–18114.
120. A. Salinas-Castillo, M. Ariza-Avidad, C. Pritz, M. Camprubi-Robles, B. Fernández, M. J. Ruedas-Rama, A. Megia-Fernández, A. Lapresta-Fernández, F. Santoyo-Gonzalez, A. Schrott-Fischer and L. F. Capitan-Vallvey, *Chem. Commun.*, 2013, **49**, 1103–1105.

121. Y. Zhou, K. J. Mintz, L. Cheng, J. Chen, B. C. L. B. Ferreira, S. D. Hettiarachchi, P. Y. Liyanage, E. S. Seven, N. Miloserdov, R. R. Pandey, B. Quiroga, P. L. Blackwelder, C. C. Chusuei, S. Li, Z. Peng and R. M. Leblanc, *J. Colloid Interface Sci.*, 2020, **576**, 412–425.
122. J. Mondal, V. Revuri, P. Choochana, P. Ganesan, W. J. Kang and Y.-K. Lee, *J. Pharm. Invest.*, 2020, **50**, 209–218.
123. S. Li, W. Su, H. Wu, T. Yuan, C. Yuan, J. Liu, G. Deng, X. Gao, Z. Chen, Y. Bao, F. Yuan, S. Zhou, H. Tan, Y. Li, X. Li, L. Fan, J. Zhu, A. T. Chen, F. Liu, Y. Zhou, M. Li, X. Zhai and J. Zhou, *Nat. Biomed. Eng.*, 2020, **4**, 704–716.
124. K. J. Mintz, G. Mercado, Y. Zhou, Y. Ji, S. D. Hettiarachchi, P. Y. Liyanage, R. R. Pandey, C. C. Chusuei, J. Dallman and R. M. Leblanc, *Colloids Surf., B*, 2019, **176**, 488–493.
125. S. Wang, L. Chen, J. Wang, J. Du, Q. Li, Y. Gao, S. Yu and Y. Yang, *Mater. Sci. Eng., C*, 2020, **116**, 111233.
126. Y. Zhang, C. Zhang, J. Chen, L. Liu, M. Hu, J. Li and H. Bi, *ACS Appl. Mater. Interfaces*, 2017, **9**, 25152–25163.
127. B. Unnikrishnan, R.-S. Wu, S.-C. Wei, C.-C. Huang and H.-T. Chang, *ACS Omega*, 2020, **5**, 11248–11261.
128. R. S. Li, P. F. Gao, H. Z. Zhang, L. L. Zheng, C. M. Li, J. Wang, Y. F. Li, F. Liu, N. Li and C. Z. Huang, *Chem. Sci.*, 2017, **8**, 6829–6835.
129. C. H. Li, R. S. Li, C. M. Li, C. Z. Huang and S. J. Zhen, *Chem. Commun.*, 2019, **55**, 6437–6440.
130. Y. Yuan, B. Guo, L. Hao, N. Liu, Y. Lin, W. Guo, X. Li and B. Gu, *Colloids Surf., B*, 2017, **159**, 349–359.
131. J. Li, M. Li, L. Tian, Y. Qiu, Q. Yu, X. Wang, R. Guo and Q. He, *Int. J. Pharm.*, 2020, **578**, 119122.
132. X.-W. Hua, Y.-W. Bao, Z. Chen and F.-G. Wu, *Nanoscale*, 2017, **9**, 10948–10960.
133. H. Cai, J. Ma, X. Xu, H. Chu, D. Zhang and J. Li, *J. Mater. Chem. B*, 2020, **8**, 5655–5666.
134. K. K. Lee, J.-G. Lee, C. S. Park, S. H. Lee, N. Raja, H.-S. Yun, J.-S. Lee and C.-S. Lee, *RSC Adv.*, 2019, **9**, 2708–2717.
135. S. Gogoi, S. Maji, D. Mishra, K. S. P. Devi, T. K. Maiti and N. Karak, *Macromol. Biosci.*, 2017, **17**, 1600271.
136. W. Chen, J. Li, Y. Xing, X. Wang, H. Zhang, M. Xia and D. Wang, *Pharm. Res.*, 2020, **37**, 134.
137. S. Sun, S. Zhao, K. Jiang, Y. Wang, Q. Shu, S. Jin, Z. Li and H. Lin, *Chem-NanoMat*, 2020, **6**, 953–962.
138. J. Yang, G. Gao, X. Zhang, Y.-H. Ma, H.-R. Jia, Y.-W. Jiang, Z. Wang and F.-G. Wu, *Nanoscale*, 2017, **9**, 15441–15452.
139. (a) M. Pei, G. Li and P. Liu, *Mater. Sci. Eng., C*, 2020, **110**, 110719; (b) G. Li, M. Pei and P. Liu, *Mater. Sci. Eng., C*, 2020, **110**, 110653.
140. G. Li, M. Pei and P. Liu, *Colloids Surf., A*, 2020, **603**, 125258.
141. M. Zhang, P. Yuan, N. Zhou, Y. Su, M. Shao and C. Chi, *RSC Adv.*, 2017, **7**, 9347–9356.
142. W. Su, R. Guo, F. Yuan, Y. Li, X. Li, Y. Zhang, S. Zhou and L. Fan, *J. Phys. Chem. Lett.*, 2020, **11**, 1357–1363.

143. C. Scialabba, A. Sciortino, F. Messina, G. Buscarino, M. Cannas, G. Roscigno, G. Condorelli, G. Cavallaro, G. Giammona and N. Mauro, *ACS Appl. Mater. Interfaces*, 2019, **11**, 19854–19866.
144. S. Sarkar, K. Das and P. K. Das, *ACS Sustainable Chem. Eng.*, 2017, **5**, 8356–8369.
145. S. D. Hettiarachchi, R. M. Graham, K. J. Mintz, Y. Zhou, S. Vanni, Z. Peng and R. M. Leblanc, *Nanoscale*, 2019, **11**, 6192–6205.
146. H.-J. Wang, X. He, T.-Y. Luo, J. Zhang, Y.-H. Liu and X.-Q. Yu, *Nanoscale*, 2017, **9**, 5935–5947.
147. S. Kim, Y. Choi, G. Park, C. Won, Y.-J. Park, Y. Lee, B.-S. Kim and D.-H. Min, *Nano Res.*, 2017, **10**, 503–519.
148. E. Ju, T. Li, Z. Liu, S. R. Da Silva, S. Wei, X. Zhang, X. Wang and S.-J. Gao, *ACS Nano*, 2020, **14**, 476–487.
149. T. S. John, P. K. Yadav, D. Kumar, S. K. Singh and S. H. Hasan, *Luminescence*, 2020, 913–923.
150. S. M. Ardekani, A. Dehghani, P. Ye, K.-A. Nguyen and V. G. Gomes, *J. Colloid Interface Sci.*, 2019, **552**, 378–387.
151. Z. Huang, T. Zhou, Y. Yuan, N. Kłodzińska, S. Zheng, T. Sternberg, C. Mørck, H. Nielsen, Y. Sun and F. Wan, *J. Colloid Interface Sci.*, 2020, **577**, 66–74.
152. S. Malmir, A. Karbalaei, M. Pourmadadi, J. Hamed, F. Yazdian and M. Navaee, *Carbohydr. Polym.*, 2020, **234**, 115835.
153. A. Roy, S. Samanta, K. Singha, P. Maity, N. Kumari, A. Ghosh, S. Dhara and S. Pal, *ACS Appl. Bio Mater.*, 2020, **3**, 3285–3293.